EARTHQUAKE INDUCED ROCK SHEAR THROUGH A DEPOSITION HOLE – PART 2

Additional calculations of the influence of inhomogeneous buffer on the stresses in the canister

Lennart Börgesson
Clay Technology AB

Jan Hernelind
5T Engineering AB

October 2013

Abstract

One extreme case of uneven density distribution of the buffer in a deposition hole have been analysed regarding the effect of a rock shear on the canister.

In the presented calculation an extreme case taken identified by Börgesson et al. (SKBdoc 1206894) and the design analysis report for the canister (Raiko et al. 2010) is modelled. This case corresponds to the worst combination of a bent (banana) shaped deposition hole and rock fall-out according to the production report of the buffer creating bending stresses on the canister (SKB 2010).

The modelling includes canisters of both PWR and BWR design. The uneven swelling pressure and the water pressure 5 MPa were applied as a total stress in the buffer before starting the shear calculation. The material models derived for the corresponding buffer densities with rate dependant stress-strain relations were used in the shear calculations.

Two cases with horizontal shear planes and different shear plane locations have been modelled; one with the shear plane in the axial midpoint of the canister and one with the shear plane in the upper ¼-point.

The results show that the modelled case yields lower stresses in both the copper shell and the cast iron insert than the corresponding base case with the density of the buffer 2050 kg/m^3 for both PWR and BWR canisters and for both cases of shear plane location.

The maximum principle stresses in the insert before shear were about 70 MPa, which is lower than the analytical results 111 MPa. This depends mainly on the smoother stress distribution in the simulation cases than applied in the simplified analytical calculation and on the copper shell that reduces and redistributes the stresses from the bentonite.

Sammanfattning

Ett extremfall av ojämn densitetsfördelning i bufferten har analyserats beträffande påverkan på kapseln av en bergskjuvning.

I denna rapport presenteras beräkningar av ett extremt fall som identifierats av Börgesson et al. (SKBdoc 1206894) och Raiko et al. (2010). Detta fall motsvarar den allvarligaste kombinationen av ett böjt (bananformat) deponeringshål och ett bergutfall beskriven i produktionslinjerapporten för bufferten (SKB 2010).

Modelleringen har omfattat kapslar av både PWR och BWR utformning. Det ojämna svälltrycket från bufferten och vattentrycket 5 MPa har applicerats som totaltryck från bufferten innan start av skjuvberäkningen. De materialmodeller som utvecklats för motsvarande buffertdensiteter och för kopparn med hastighetsberoende spännings-töjningssamband har även använts i dessa skjuvberäkningar.

Två fall med horisontella skjuvplan och olika positioner av skjuvplanen har modellerats; ett med skjuvplanet i centrum av kapseln och ett med skjuvplanet i övre ¼-delspunkten.

Resultaten visar att de modellerade fallen ger lägre spänningar både i kopparhöljet och i segjärnsinsatsen än motsvarande normalfall med buffertdensiteten 2050 kg/m^3 både för PWR och BWR-kapslarna och för båda skjuvplanspositionerna.

Den största huvudspänningen i insatsen innan skjuvning blev för de modellerade fallen 70 MPa, vilket är lägre än 111 MPa som räknades fram med förenklade analytiska metoder. Anledningen är i huvudsak att spänningsfördelningen från bentoniten är jämnare i de numeriska beräkningarna än de som ansattes i de analytiska beräkningarna och framförallt att kopparhöljet reducerar och omfördelar spänningarna från bentoniten.

Contents

1 Introduction

1.1 Background

The calculation method and material models used for modelling a rock shear through a deposition hole have been developed and verified in a number of reports and used in the global modelling of the canister in a deposition hole. See e.g. Dueck et al. (2010), Börgesson et al. (2010), Börgesson and Hernelind (2010) and Hernelind (2010). These calculations are based on the assumption that the buffer is completely water saturated and homogeneous with uniform density.

The case of uneven swelling pressure caused by unfavourable rock surface contour of the deposition hole was not combined with the rock shear case in the design analysis report for the canister (Raiko et al. 2010).

In the calculation described in this report an extreme case taken from SKBdoc 1206894 and the design analysis report for the canister (Raiko et al. 2010) is modelled. This case corresponds to the worst combination of banana shaped deposition hole and rock fall-out according the production report of the buffer (SKB 2010).

1.2 Scope of modelling

The modelling includes both PWR and BWR canisters. The uneven swelling pressure and the water pressure 5 MPa were applied as a resulting total stress in the buffer before starting the shear simulation. The material models derived for the corresponding buffer densities with rate dependant stress-strain relations were used in the shear calculations.

The results of the shear calculations are compared to corresponding calculations of the highest allowed density of the buffer 2050 kg/m^3. The stresses in the insert before shear are also compared to corresponding analytical estimations done by Börgesson et al. (SKBdoc 1206894).

1.3 Data storage

The input files, geometry definitions and script files are stored at SKB. The names of the files are given in Appendix 1.

2   Modelling case

The modelled case is the case that gives the highest stresses in the insert, which corresponds to case 1+2 by Börgesson et al. (SKBdoc 1206894). Figure 2-1 shows the geometry.

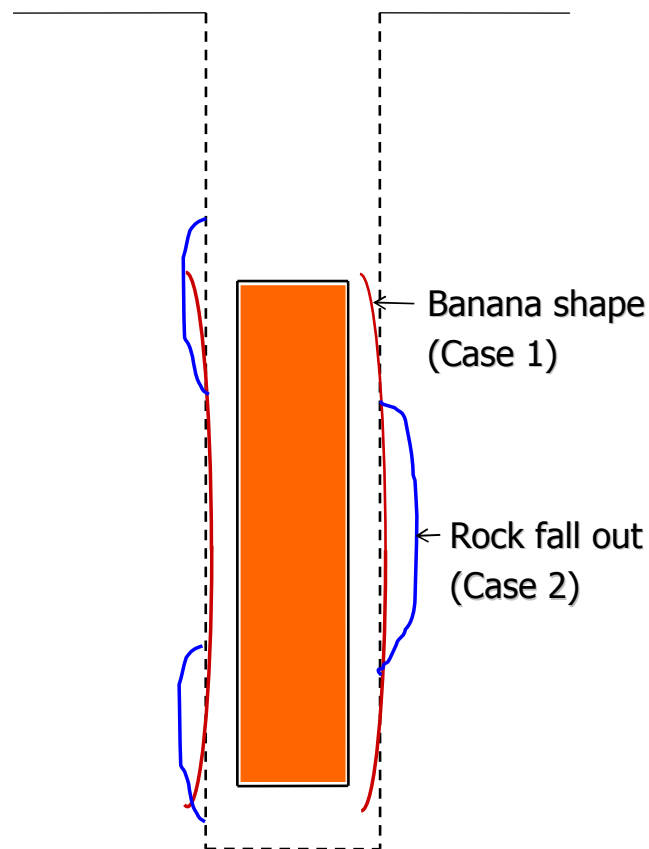A combination of cases 1 and 2 yields the load case shown in Figure 2-2.

Figure 2-1. The two combined cases 1 and 2 of deformed rock contours. The read lines illustrate a banana-shaped hole and the blue lines illustrate rock fallouts that accentuate the banana shape.
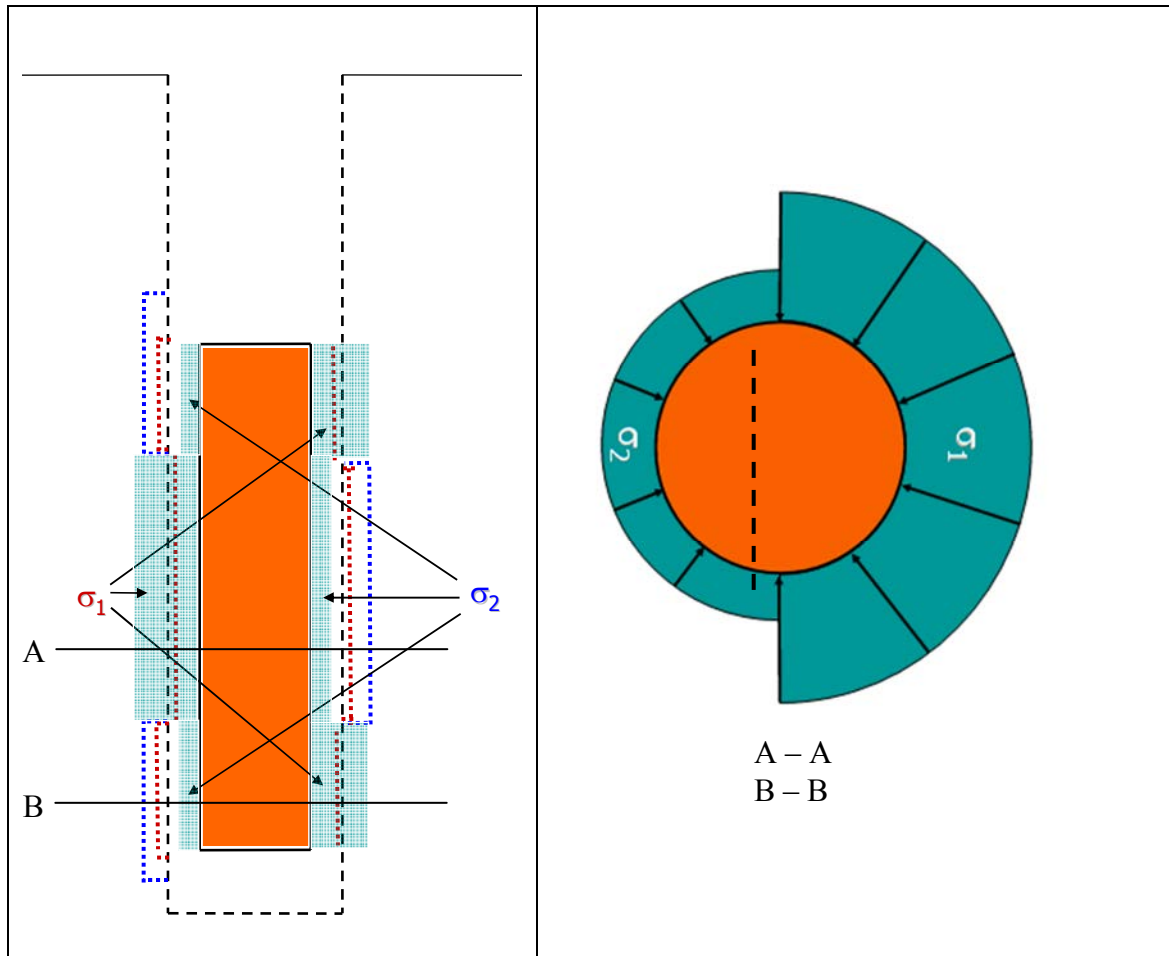
Figure 2-2. *The combined load case 1+2 used in the calculation. The right figure refers to section B-B and mirrored for section A-A.*

The following densities at saturation correspond to this combined load case (SKBdoc 1206894):

ρ_1=2021 kg/m^3
ρ_2=1959 kg/m^3

which yield the swelling pressures

σ_1=7 823 kPa
σ_2=3 727 kPa

In addition to these swelling pressures the water pressure 5 MPa will be added.

The following two densities, which are close to the ones given in SKBdoc 1206894, are used in the calculations since material models for those densities have been derived (Börgesson et al. 2010):

ρ_1=2020 kg/m^3
ρ_2=1970 kg/m^3

This density distribution along the canister continues also below and above the canister i.e. the left half of the hole (in Figure 2-2) has the density 1970 kg/m^3 and the right half has the density 2020 kg/m^3 both above and below the canister

The actual differences in rock geometry from the original case are not included in the model since they are too small to significantly influence the results. The effect of the hole geometry is considered to be reflected in the inhomogeneity of the buffer and hence the model has a straight deposition hole.

The canister geometries are identical to the geometries of PWR and BWR canisters (SKBdoc 1203875, SKB 2010)

The shear plane is horizontal and two cases with different locations have been studied. In the first case the shear plane is located in the centre of the canister and in the second case the shear plane is located in the upper ¼-pont of the canister. The applied shear rate is 1 m/s and the shear are driven to 5 cm and 10 cm in two steps.

3 Material models

3.1 General

The finite element code Abaqus has been used for the calculations. The materials have been modelled as elastic-plastic materials with stress-strain properties that correspond to the different materials and the shear rate applied. The material models and the calculation technique have gradually been improved as a consequence of improved knowledge in concordance with the modelling of the actual rock shear cases for SR-Site.

3.2 Bentonite model

The bentonite is modelled with identical models as used for the SR-Site calculations but adapted to the bentonite used in three scale tests, the actual density of the bentonite and to the actual strain rate. The scale tests and the modelling of the scale tests are described in Börgesson and Hernelind (2010). The material model is described in Börgesson et al. (2010) and Börgesson and Hernelind (2010). The bentonite buffer is modelled using only total stresses that don't include the pore water pressure, the reason being the very fast compression and shear. The stress-strain relation is in Abaqus expressed with von Mises stress σ_j that describes the "shear stress" in three dimensions according to Equation 3-1.

$$\sigma_j = (((\sigma_1 - \sigma_3)^2 + (\sigma_1 - \sigma_2)^2 + (\sigma_2 - \sigma_3)^2)/2)^{1/2} \tag{3-1}$$

where

σ_1, σ_2 and σ_3 are the major principal stresses.

At triaxial tests σ_2 and σ_3 are equal and the Mises stress equal to the deviator stress q.

$$q = (\sigma_1 - \sigma_3) \tag{3-2}$$

The stress-strain properties of bentonite have been investigated in several laboratory studies. The results of the studies and the resulting material model used for SR-Site are described in two separate reports (Börgesson et al. 2010, Dueck et al. 2010). The material used for the modelling in SR-Site differs from the material used for the scale tests, since MX-80Ca (MX-80 ion-exchanged from Na-bentonite to Ca-bentonite) is used as reference buffer material in SR-Site while unaffected MX-80 was used in the scale tests.

Relation between shear strength and density

The most important property of the buffer in a rock shear scenario is the shear strength since the shear strength limits the stiffness of the buffer. When the shear strength is

reached the buffer can be plastically deformed without additional stresses. The higher the shear strength of the buffer is the higher the stresses will be in the canister.

The shear strength of MX-80 has been measured at different densities at different conditions. Figure 3-1 shows the results together with measurements on Ca-bentonites. See Börgesson et al. (2010) and Dueck et al. (2010). The void ratio *e* is used in the figure instead of the density at water saturation since Abaqus uses void ratio as variable. The void ratio is defined as the ratio between the volume of the voids and the volume of the solids and can be calculated from the density according to Equation 3-3.

$$e = \frac{\rho_s - \rho_m}{\rho_m - \rho_w}$$

$$(3-3)$$

where

ρ_s = density of solids = 2 780 kg/m^3 (Karnland et al. 2006)
ρ_m = density at water saturation
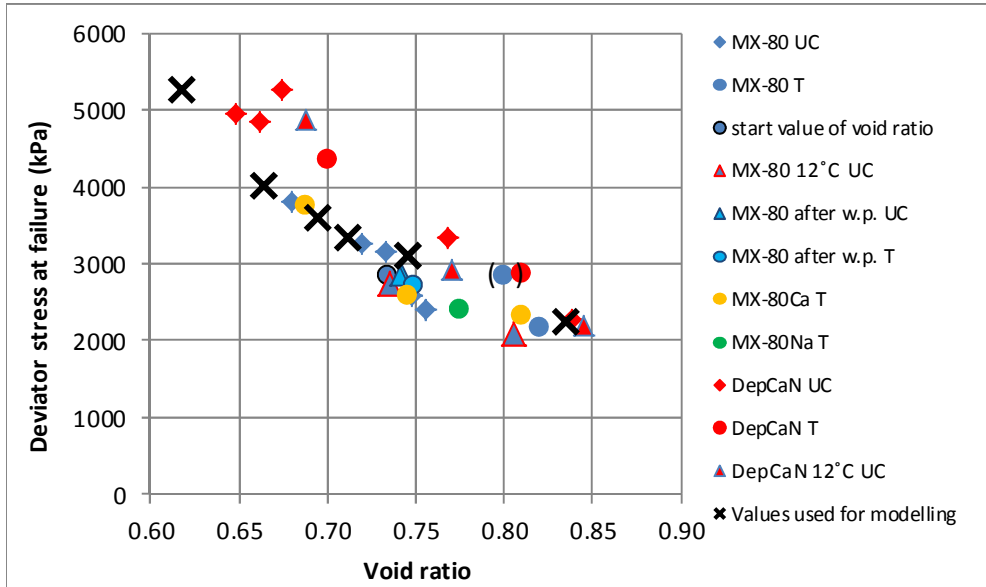ρ_s = density of water = 1 000 kg/m^3

Figure 3-1. *Measured deviator stress at failure as a function of void ratio for different bentonites at different test techniques. The relation used for MX-80 in the calculations is marked with x and relates to the strain rate 10^{-4} s^{-1}. For information about the legend of the different test results; see Dueck et al. (2010).*

Relation between shear strength and strain rate

The shear strength of bentonite is as for many materials dependant on the strain rate. Investigations of the influence of strain rate have yielded a dependency described by Equation 3-4 (Börgesson et al. 2010).

$$q_{fs} = q_{fs0} \left(\frac{v_s}{v_{s0}} \right)^n$$

$$(3-4)$$

where

v_s = strain rate
v_{s0} = reference strain rate = 10^{-4} 1/s
q_{fs} = deviator stress at failure at the strain rate v_s
q_{fs0} = deviator stress at failure at the reference strain rate v_{s0}
n = 0.038

The value n=0.038 has been found valid for MX-80 and some other bentonites and has been used for SR-Site.

Applying the relation between shear strength q_{fs0} and void ratio at the strain rate v_{s0} = 10^{-4} according to the x-marks in Figure 3-1, Equation 3-4 thus yields the shear strength of the material at different strain rates and void ratios.

Stress-strain relation

Numerous triaxial and uniaxial tests have shown that the stress-strain relation during shear is very similar if the deviator stress (Mises stress) is normalised against the strength (maximum deviator stress). This means that both the elastic and the plastic parts are proportional to the actual strength. A general stress-strain relation for uniaxial unconfined compression with the following properties has been derived for SR-Site (Börgesson et al. 2010):

- Linear elastic in the strain interval $0 < \varepsilon <\approx 1\%$ with an elasticity that yields 58% of the maximum Mises stress at the strain $\varepsilon \approx 1\%$
- Plastic hardening in the strain interval $\approx 1\% < \varepsilon <\approx 5.3\%$ with the maximum Mises stress determined according to the relation in Figure 3-1
- Almost ideally plastic at $\varepsilon >\approx 5.3\%$

For the buffer material with the density at saturation ρ_m = 2020 kg/m^3 (e=0.745) at the reference strain rate (v_{s0} = 10^{-4} s^{-1}) this yields an E-modulus of E=179 MPa and a maximum Mises stress of q_{fs0} = 3.10 MPa at the strain $\varepsilon >5.4\%$.

The shear takes place at such a high rate that no pore water transport can occur during the shear, which means that no volume change of the water saturated material can take place. Thus Poisson's ratio must be close to 0.5, corresponding to no volume change. However, a small amount of volume change will appear due to compressibility of water and therefore Poisson's ratio has been chosen to

$v = 0.49$

in all calculations.

Elastic-plastic stress-strain relation

The stress-strain relation can be achieved with an elastic-plastic material model according to Table 3-1.

Table 3-1. Elastic-plastic material data for the bentonite buffer at one density and one strain rate.

Mate-rial	ρ_m kg/m³	Rate of strain v_s s⁻¹	Elastic part		Plastic part: von Mises true stress σ_j (MPa) at the following plastic nominell strains ε_p							
			E MPa	v	$\varepsilon_p=$ 0	$\varepsilon_p=$ 0.004	$\varepsilon_p=$ 0.01	$\varepsilon_p=$ 0.018	$\varepsilon_p=$ 0.026	$\varepsilon_p=$ 0.036	$\varepsilon_p=$ 0.46	$\varepsilon_p=$ 1.0
MX-80	2 020	10⁻⁴	179	0.49	1.79	2.39	2.75	2.93	3.06	3.10	3.06	3.06

Since the elastic strain is added to the plastic strain the total strain at the maximum Mises stress will be $\varepsilon =5.4\%$.

By applying the influence of the strain rate according to Equation 3-4 new values of the maximum Mises stress and corresponding data for the elastic plastic material model can be derived for other strain rates. Table 3-2 shows the results as a table with strain rates varying between 10^{-6} s⁻¹ and 10^3 s⁻¹. Linear interpolation is applied between the tabulated values.

Abaqus has a unique feature that allows for assigning individual strain rate dependent properties. The plastic properties of each element can be made a function of the strain rate of the element. However, this feature does not allow for changes in elastic properties but only plastic, so a constant elasticity must be used. Since the elasticity only affects the strain at failure the E-modulus of an average strain rate ($v_s =0.1$ s⁻¹) has been used in the calculation which makes the strain at failure to be between about 4.5% and 6.0%. The resulting stress-strain relations at different strain rates are plotted in Figure 3-2.

Corresponding properties at the density 2020 kg/m³ has been derived in an identical way. The resulting material model is shown in Table 3-3 and Figure 3-3.

Table 3-2. Elastic-plastic material data for the bentonite buffer at the density 2 020 kg/m^3 (e=0.745) and all strain rates.

| Mate-rial	ρ_m kg/m^3	Rate of strain v_s s^{-1}	Elastic part E MPa	ν	$\varepsilon_p=$ 0	$\varepsilon_p=$ 0.004	$\varepsilon_p=$ 0.01	$\varepsilon_p=$ 0.018	$\varepsilon_p=$ 0.026	$\varepsilon_p=$ 0.036	$\varepsilon_p=$ 0.46	$\varepsilon_p=$ 1.0
					Plastic part: von Mises true stress σ_j (MPa) at the following plastic nominal strains ε_p							
MX-80	2 020	10^{-6}	150	0.49	1.50	2.01	2.30	2.46	2.56	2.60	2.57	2.57
MX-80	2 020	10^{-4}	179	0.49	1.79	2.39	2.75	2.93	3.06	3.10	3.06	3.06
MX-80	2 020	10^{-3}	195	0.49	1.95	2.61	2.99	3.20	3.33	3.38	3.34	3.34
MX-80	2 020	10^{-2}	213	0.49	2.13	2.85	3.27	3.49	3.64	3.69	3.65	3.65
MX-80	2020	10^{-1}	233	0.49	2.33	3.11	3.57	3.81	3.97	4.03	3.98	3.98
MX-80	2 020	1.0	254	0.49	2.54	3.39	3.90	4.16	4.34	4.40	4.35	4.35
MX-80	2 020	10	277	0.49	2.77	3.70	4.25	4.54	4.73	4.80	4.74	4.74
MX-80	2 020	100	303	0.49	3.03	4.04	4.64	4.96	5.16	5.24	5.18	5.18
MX-80	2 020	1000	330	0.49	3.30	4.41	5.07	5.41	5.64	5.72	5.65	5.65
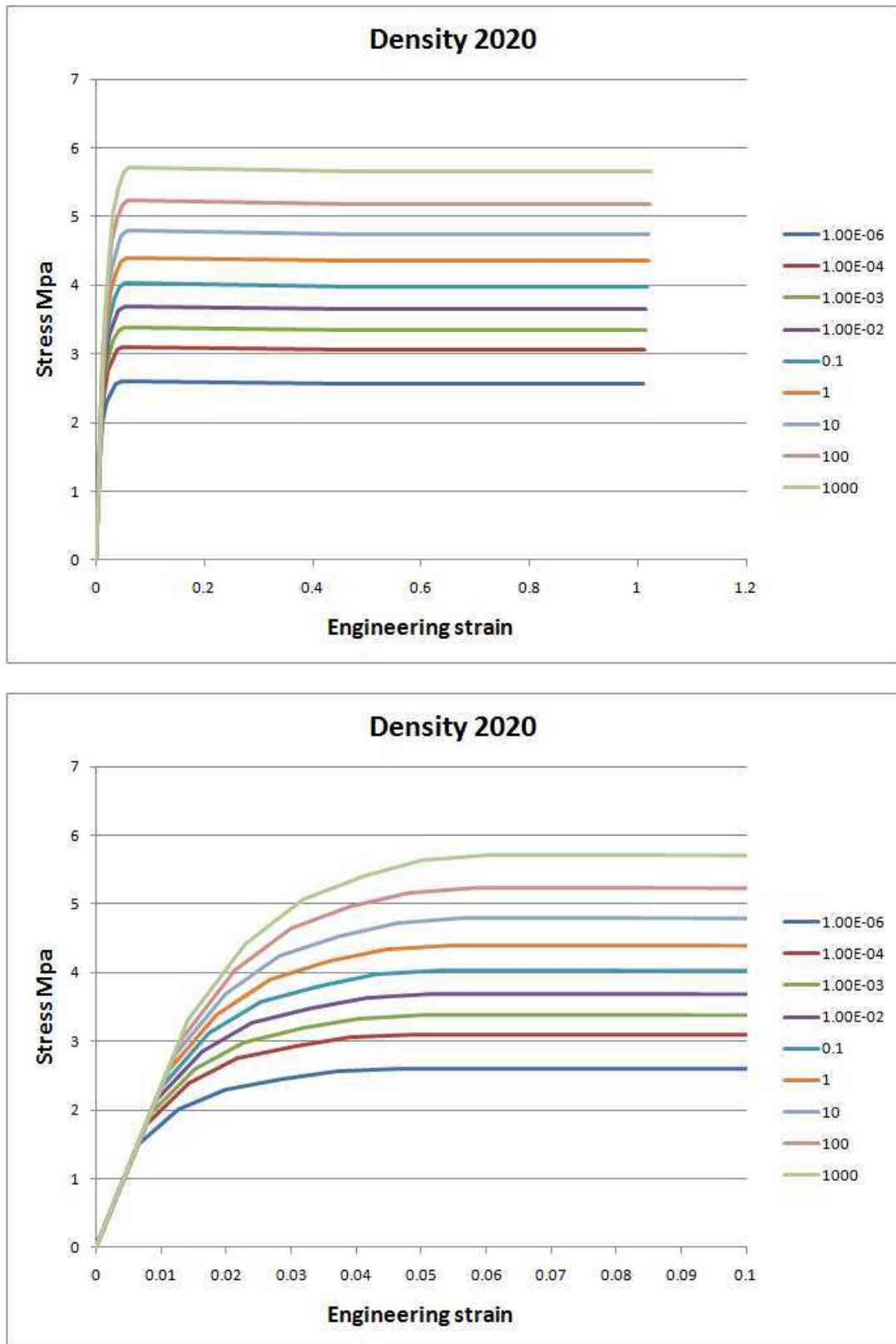
Figure 3-2. Stress-strain model of MX-80 bentonite at different strain rates (s^{-1}) at the density at saturation 2020 kg/m^3 plotted as Mises stress as function of the engineering strain.

Table 3-3. Bentonite model (MX-80) at the density 1970 kg/m^3 (e=0.835).

Material	ρ_m kg/m^3	Rate of strain v_s s^{-1}	Elastic part		Plastic part: von Mises true stress σ_j (MPa) at the following plastic nominell strains ε_p							
			E MPa	v	ε_p= 0	ε_p= 0.004	ε_p= 0.01	ε_p= 0.018	ε_p= 0.026	ε_p= 0.036	ε_p= 0.46	ε_p= 1.0
MX-80	1 970	10^{-6}	109	0.49	1.09	1.46	1.67	1.79	1.86	1.89	1.87	1.87
MX-80	1 970	10^{-4}	130	0.49	1.30	1.74	2.00	2.13	2.23	2.25	2.23	2.23
MX-80	1 970	10^{-3}	142	0.49	1.42	1.90	2.17	2.33	2.42	2.46	2.43	2.43
MX-80	1 970	10^{-2}	155	0.49	1.55	2.07	2.38	2.54	2.65	2.68	2.65	2.65
MX-80	1 970	10^{-1}	169	0.49	1.69	2.26	2.60	2.77	2.89	2.93	2.89	2.89
MX-80	1 970	1.0	185	0.49	1.85	2.47	2.84	3.03	3.16	3.20	3.16	3.16
MX-80	1 970	10	201	0.49	2.01	2.69	3.09	3.30	3.44	3.49	3.45	3.45
MX-80	1 970	100	220	0.49	2.20	2.94	3.37	3.61	3.75	3.81	3.77	3.77
MX-80	1 970	1000	240	0.49	2.40	3.21	3.69	3.93	4.10	4.16	4.11	4.11
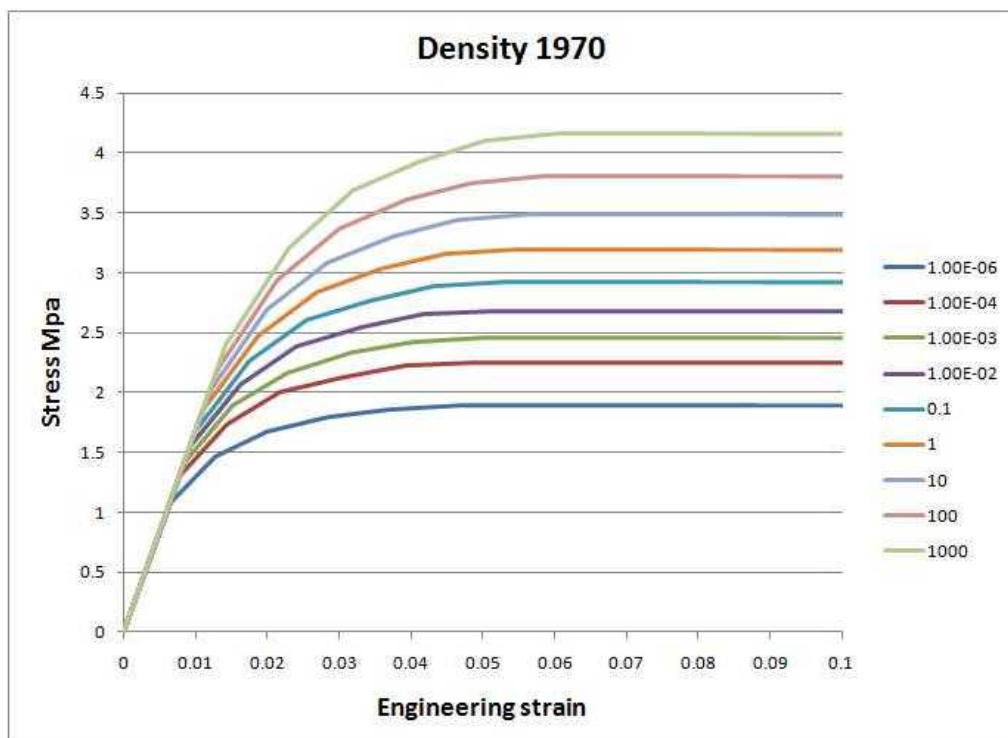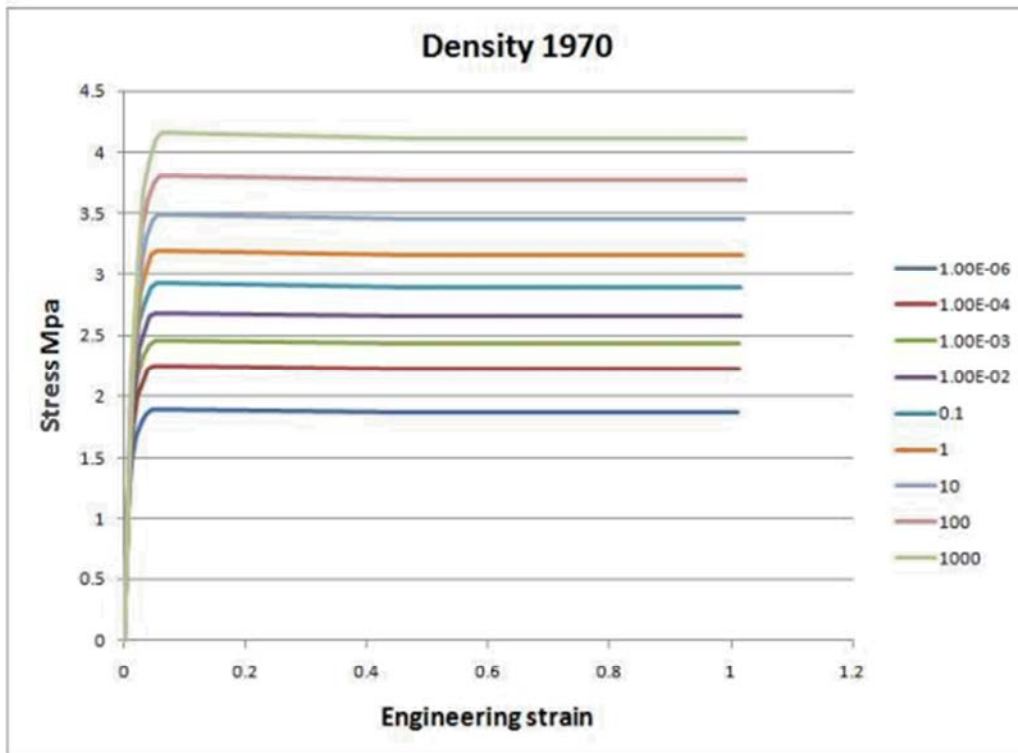
Figure 3-3. *Stress-strain model of MX-80 bentonite at different strain rates (s^{-1}) at the density at saturation 1970 kg/m^3 plotted as Mises stress as function of the engineering strain.*

3.3   Copper model

The material model used for copper is described below.

The stress-strain properties of the copper in the copper shell were investigated by the Corrosion and metals research institute Swerea Kimab and the results were then represented by a creep material model developed by Rolf Sandström, see Sandström and Andersson (2008), Jin and Sandström (2008, 2009) and Sandström et al. (2009).

The material model for the short duration rock shear analysis is based on a simplified elastic-plastic material model, see Table 3-4, using data from the creep model assuming a strain rate of 0.005/s which is considered as conservative.

The flow curve data has been calculated from Sandström et al. (2009) wherein eq.(17) has been used together with the parameter values defined in the corresponding Table 4-2, as well as $m = 3.06$, $\alpha = 0.19$, $\omega = 14.66$. See the referred document for further description.

The copper model data is shown in Figure 3-4. Data is available up to 50 % and covers the range of obtained results.

Table 3-4. Elastic-plastic material data for the copper at strain rate 0.005/s.

Elastic part		Plastic part: von Mises stress σ_j (MPa) at the following plastic strains (ε_p)					
E (MPa)	ν	0	0.10	0.20	0.30	0.40	0.50
$1.2 \cdot 10^5$	0.308	72	178	235	269	288	300
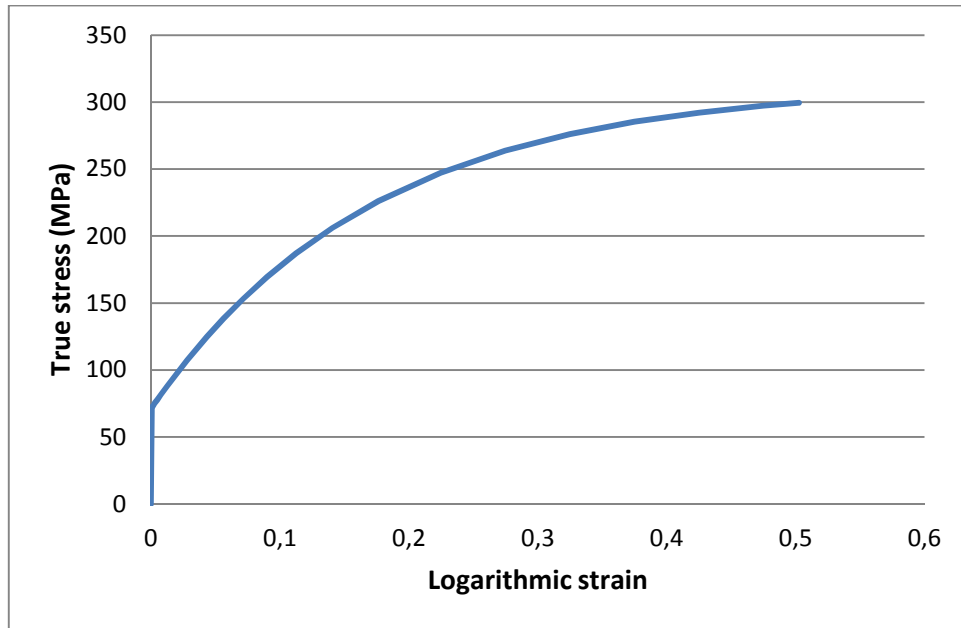
Figure 3-4. *The copper shell material model gives the true stress [MPa] as a function of the logarithmic strain.*

3.4 Contact surfaces

All the boundaries of the bentonite against the copper canister are equipped with contact surfaces. All contact surfaces have friction at sliding along the elements with no cohesion and the friction coefficient 0.1, i.e. the friction angle and cohesion are

$\phi = 5.7°$

c=0 kPa

The contact is thus released when the swelling pressure is lost.

The low friction angle was used at the earlier calculations and corresponds to about half the friction angle of the material at the actual densities, which has been shown to be valid for metal/bentonite contacts. See e.g. Börgesson et al. (1995).

4   Calculations

4.1   General

The FE-model consists of the insert (PWR or BWR-design) made by nodular cast iron, the lid on the top of the insert made by steel, the surrounding copper shell surrounded by the buffer made by bentonite. The two models are identical except for the insert.

4.2   Element mesh

4.2.1   Assembly

The assembled entire model is built by about 135000 elements (about 160000 nodes), mainly 8-node hexahedron elements, see Fig 4-1.
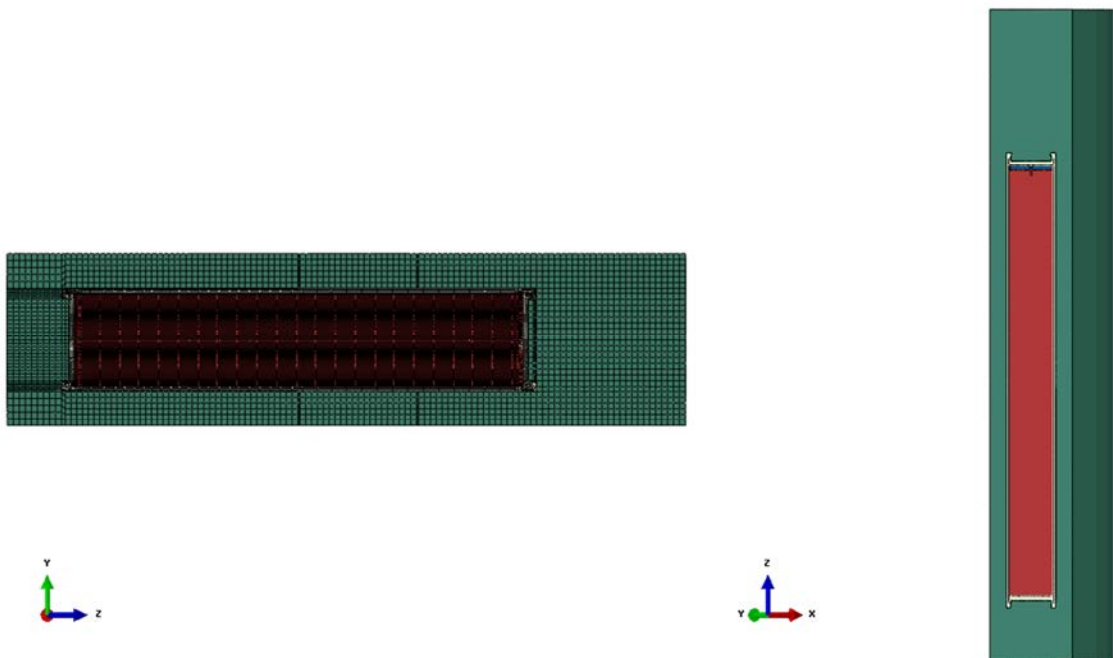
Figure 4-1. *Plot showing the entire assembly and the mesh. The two shear planes are indicated in the left figure.*

4.2.2   Buffer (bentonite)

The buffer consists of about 35000 elements (41000 nodes), 8-noded hexahedron elements with reduced integration, see Fig 4-2.
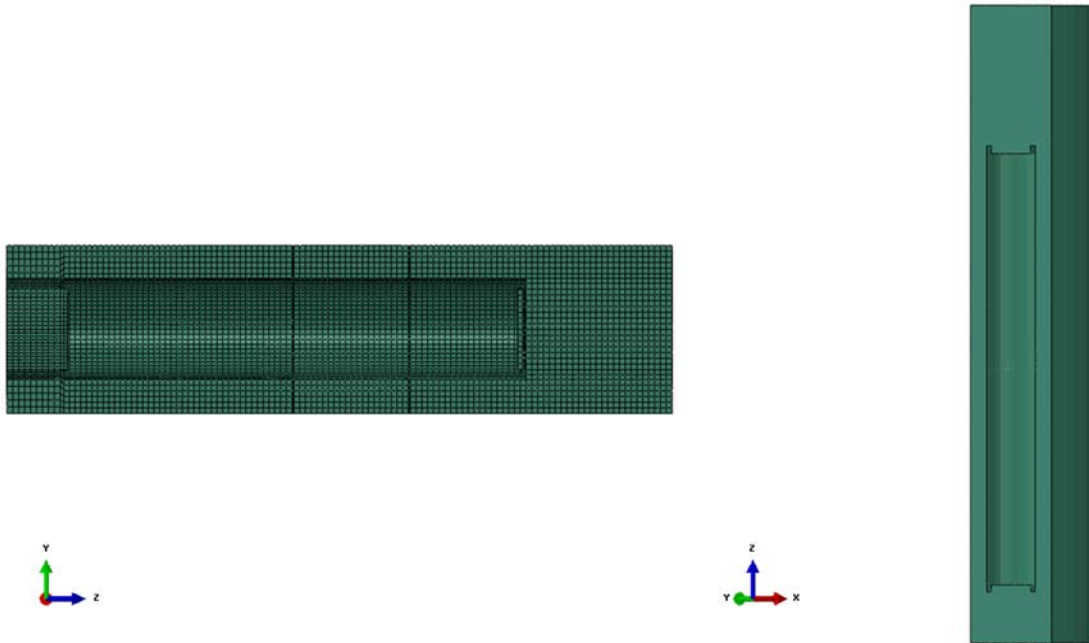
Figure 4-2. *Plot showing the buffer and the mesh. The two shear planes are indicated in the left figure.*

4.2.3   Copper shell

The copper shell consists of about 30000 elements (37000 nodes), 8-noded hexahedron elements using full integration, see Fig 4-3.
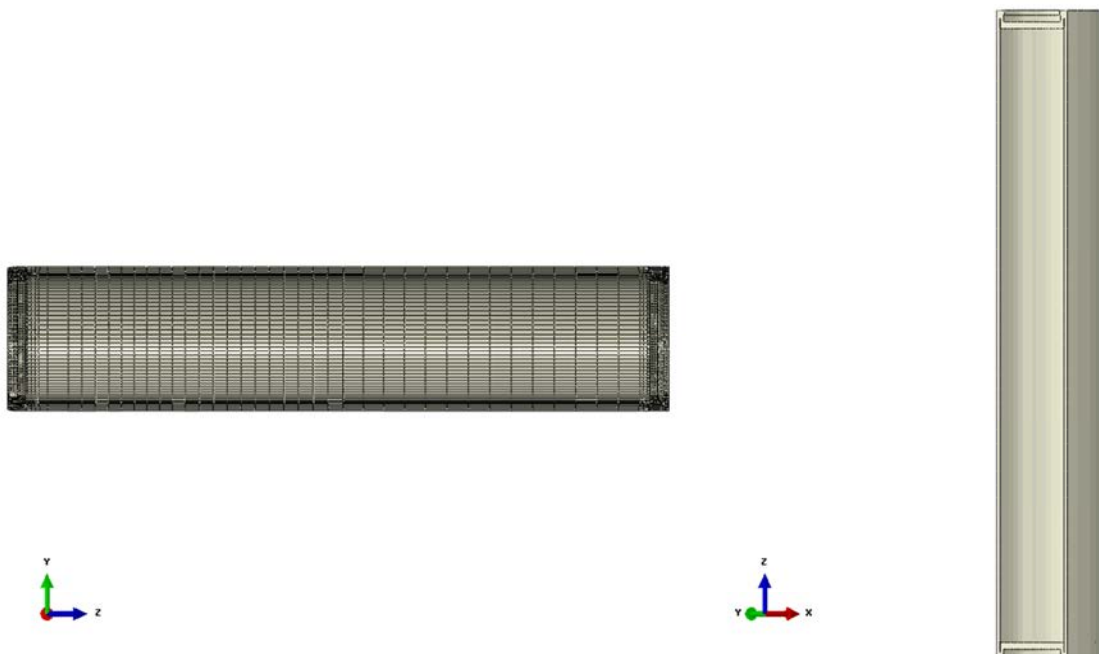
Figure 4-3. *Plot showing the copper shell and the mesh.*

4.2.4 Lid (made of steel)

The steel lid consists of about 1100 elements (1800 nodes), 8-noded hexahedron using reduced integration, see Fig 4-4.
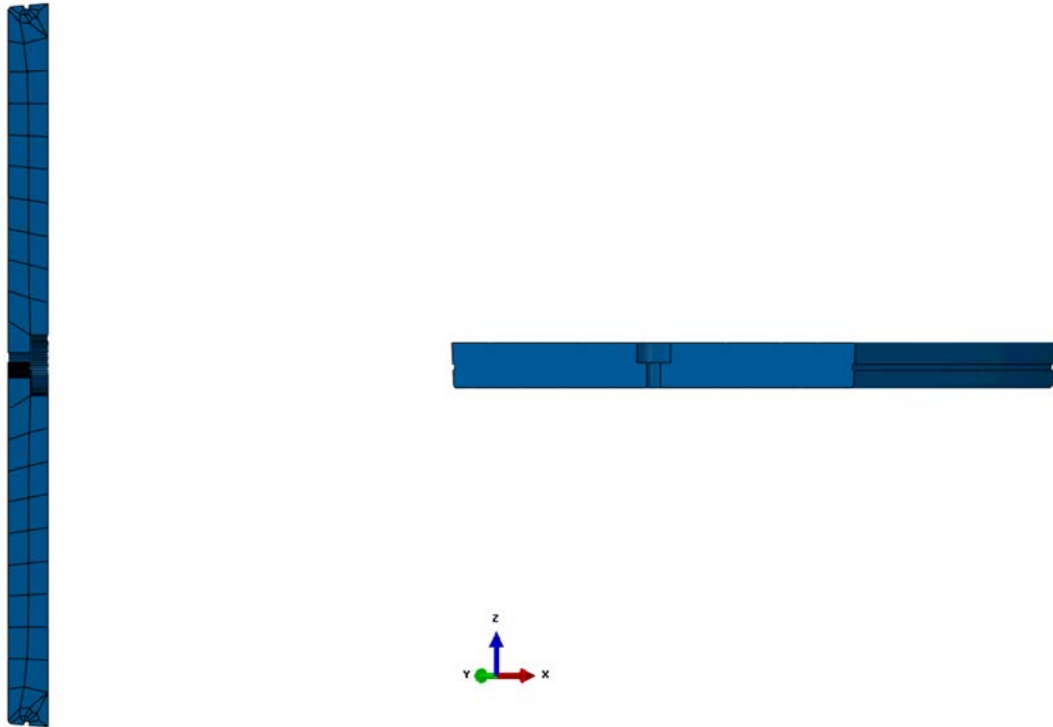
Figure 4-4. *Plot showing the steel lid and the mesh.*

4.2.5 BWR-insert (made of nodular cast iron)

The BWR-insert consists of about 70000 elements (80000 nodes), 8-noded hexahedron elements using reduced integration or full integration and a few 6-noded wedge elements, see Fig 4-5.
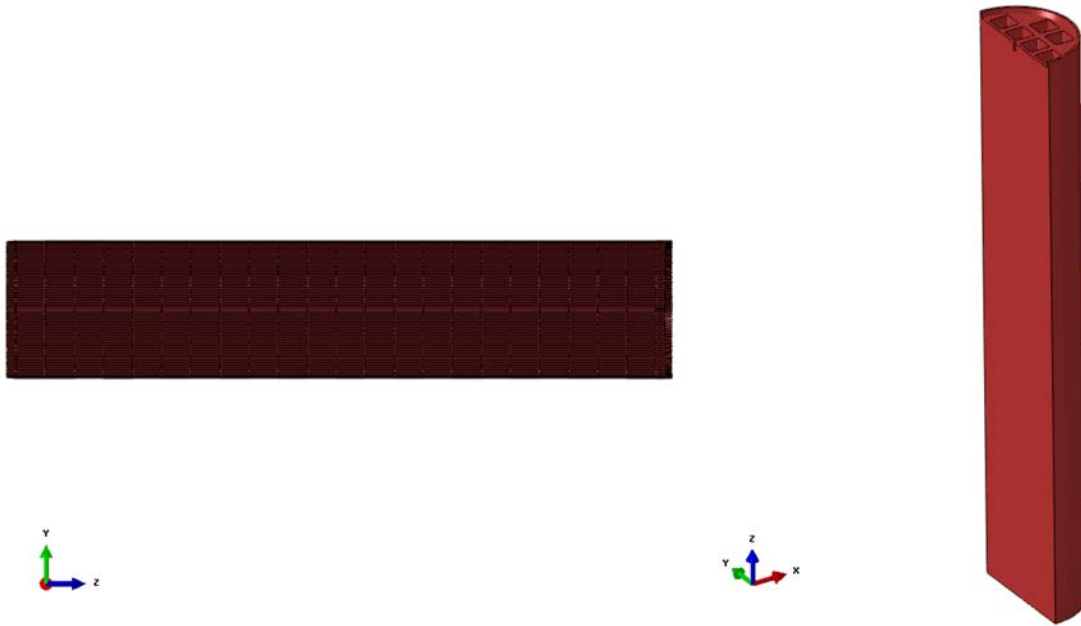
Figure 4-5. *Plot showing the BWR-insert and the mesh.*

4.2.6   PWR-insert (made of nodular cast iron)

The PWR-insert consists of about 29000 elements (34000 nodes), 8-noded hexahedron elements using reduced integration or full integration and a few 4-noded wedge elements, see Fig 4-6. The cassette tubes have been modelled as a part of the PWR insert as a partition with a separate material model corresponding to a welded connection.
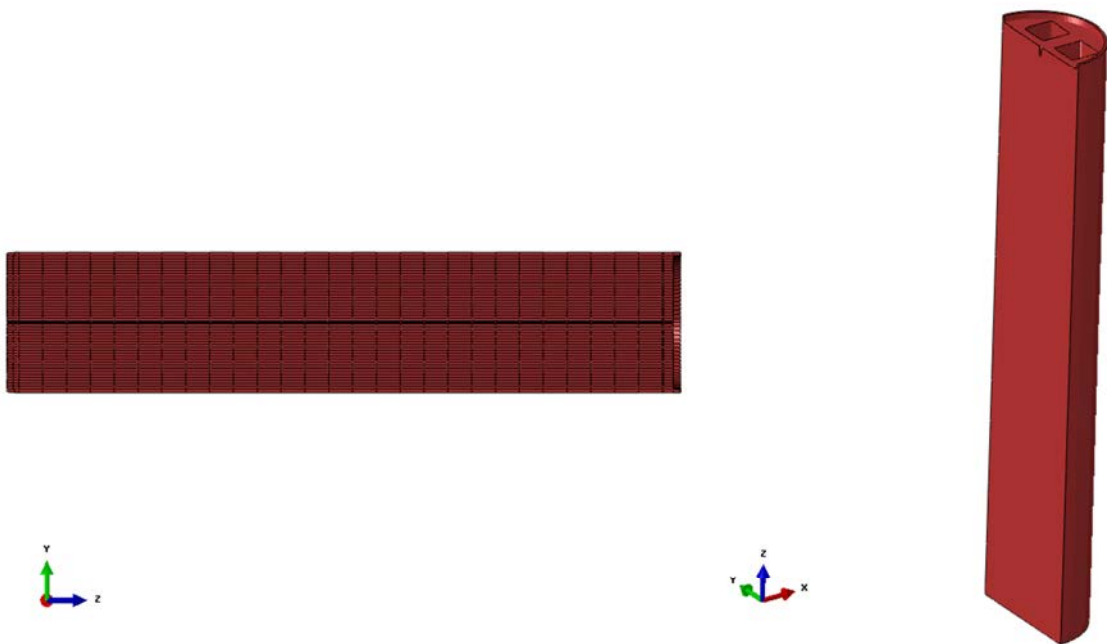
Figure 4-6. *Plot showing the PWR-insert and the mesh.*

4.3   Method of calculation

The performed analyses consist of three steps:

- Step1 consists of application of the gravity load (the initial swelling pressure plus water pressure) in the buffer

- Step2 consists of a following prescribed horizontal shearing displacement (5 cm) at the mid section respectively at the upper ¼-point.

- Step3 consists of additional horizontal displacement (5 cm) at the mid section respectively at the upper ¼-point.

The results will be compared also with previous performed hand-calculations and thus it is important to have the initially applied swelling pressure as close as possible to the pressure distribution used at the hand-calculations, which was assumed to be the most critical (and possible) swelling pressure distribution.

Since the analyses are performed based on total stresses, the swelling pressure plus water pressure is simulated by prescribing initial conditions for the stresses in the buffer. However, the insert will be deformed when these stresses are applied and furthermore the insert has a stiffness which varies making the process to have the correct initial swelling pressure plus water pressure difficult. The buffer has been divided in 6 regions with different magnitude and distribution of the initial applied stresses - totally 10 parameters which have to be tuned.

5   Results

5.1   General

The results from three different calculation steps are presented. At first the swelling pressure and the resulting stresses in the bentonite on the canister and the stresses in the canister are shown. Then the results from the shear displacement 5 cm and 10 cm are shown.

The results are compared with the results from the earlier simulation with a uniform density of 2050 kg/m^3 of the buffer (Hernelind 2010). This case is referred as the base case.

Two locations of the horizontal shear plane have been modelled, in the centre and in the upper ¼ point of the canister.

5.2   Initial stresses before shear

The initial stresses are applied in two steps. Since the stiffness of the bentonite is much higher in the material model than what corresponds to the swelling capacity of the bentonite the initial stress in the bentonite must be much higher than the final desired swelling pressure plus water pressure on the canister. The small deformations of especially the copper shell is enough to reduce the stress significantly. An iterative procedure had to be applied in order to get the correct stresses on the canister (see section 4.3). Figure 5-1 shows the initial stress and the final stresses on the canister after equilibrium.
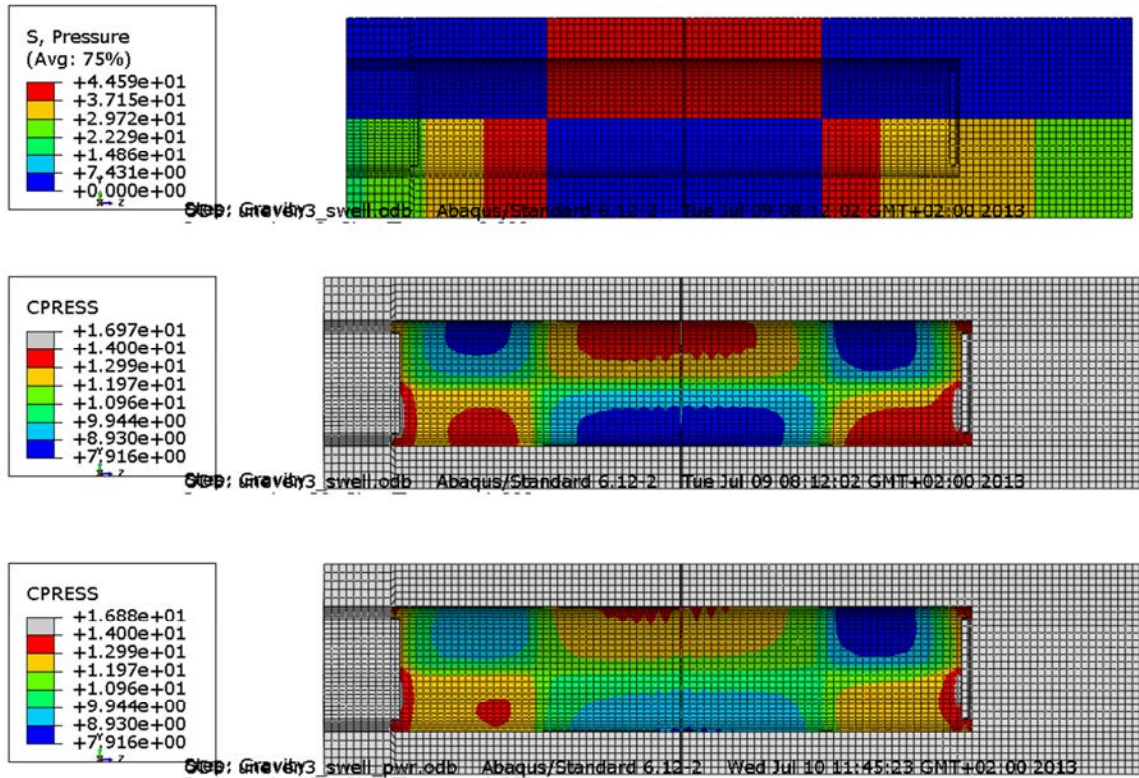
Figure 5-1. *Initial stresses [MPa] in the bentonite before equilibrium (upper picture) and the contact stresses on the canister after equilibrium for the canister with BWR insert (middle) and PWR insert (lower).*

The results show that the calculated contact stresses are similar to the desired stress (plus the water pressure 5 MPa) but the stress transition is much smoother than in the original model used for the analytical calculation (see Figure 2-2).

Figure 5-2 to 5-4 shows the resulting stresses after equilibrium in the BWR insert and comparison with the stresses in the base case. Figure 5-2 shows the Mises stresses, Figure 5-3 shows the axial stresses and Figure 5-4 shows the maximum principal stresses.

Figure 5-5 shows the plastic strain in the copper shell.
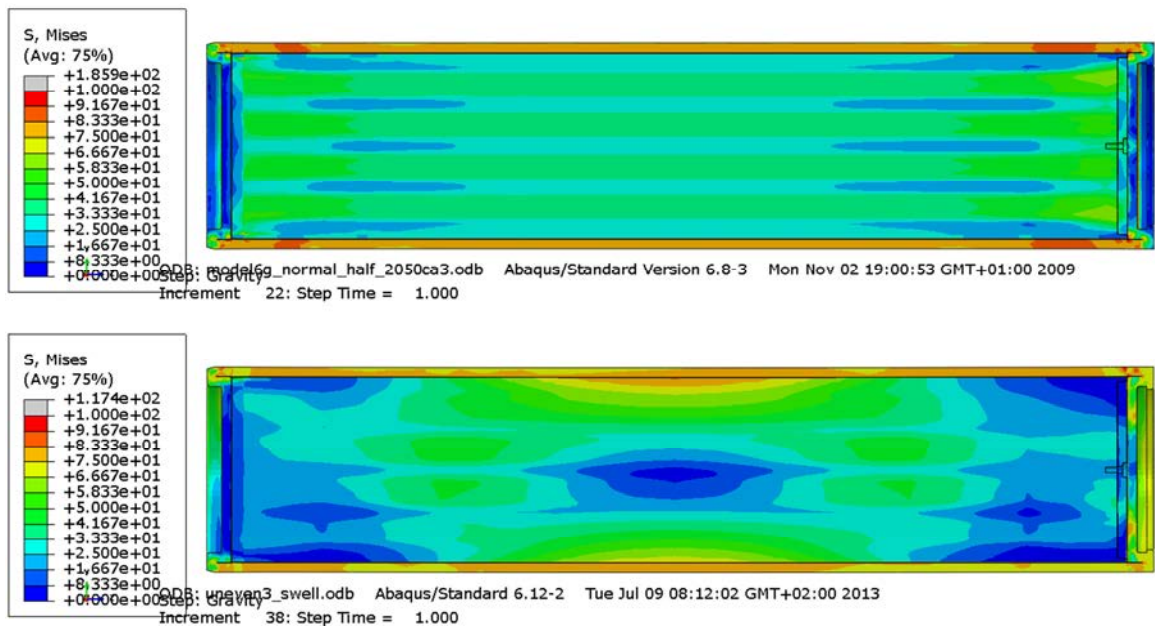
Figure 5-2. *Mises stress (MPa) in the BWR insert (upper: base case).*
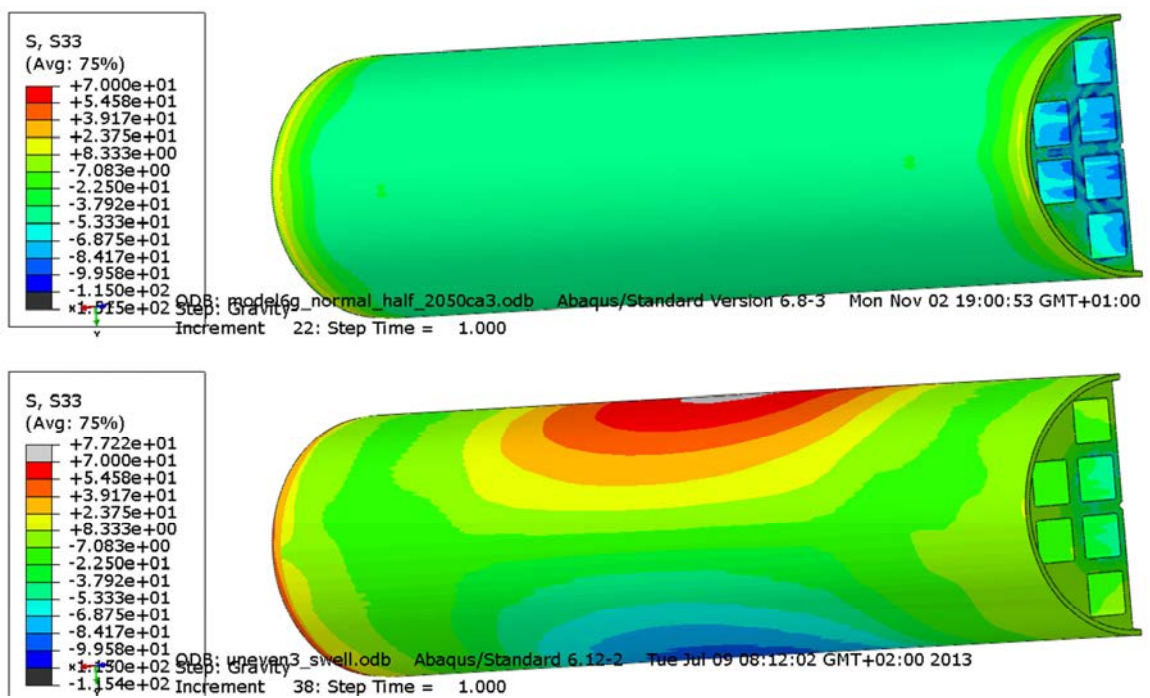
Figure 5-3. *Axial stress (MPa) in the BWR insert (upper: base case).*
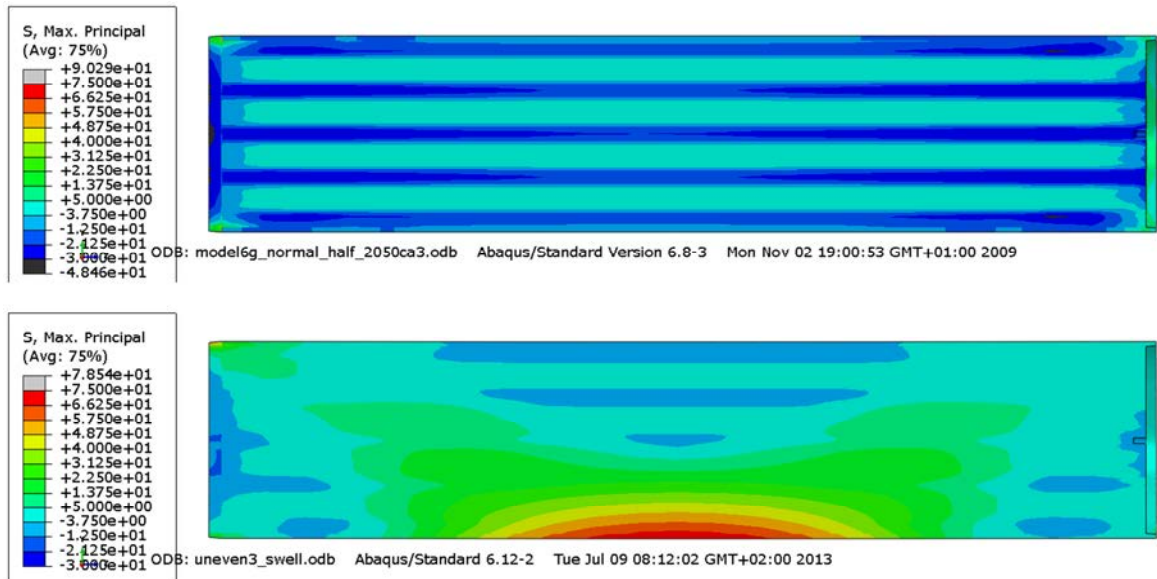
Figure 5-4. *Maximum principal stress (MPa) in the BWR insert (upper: base case).*
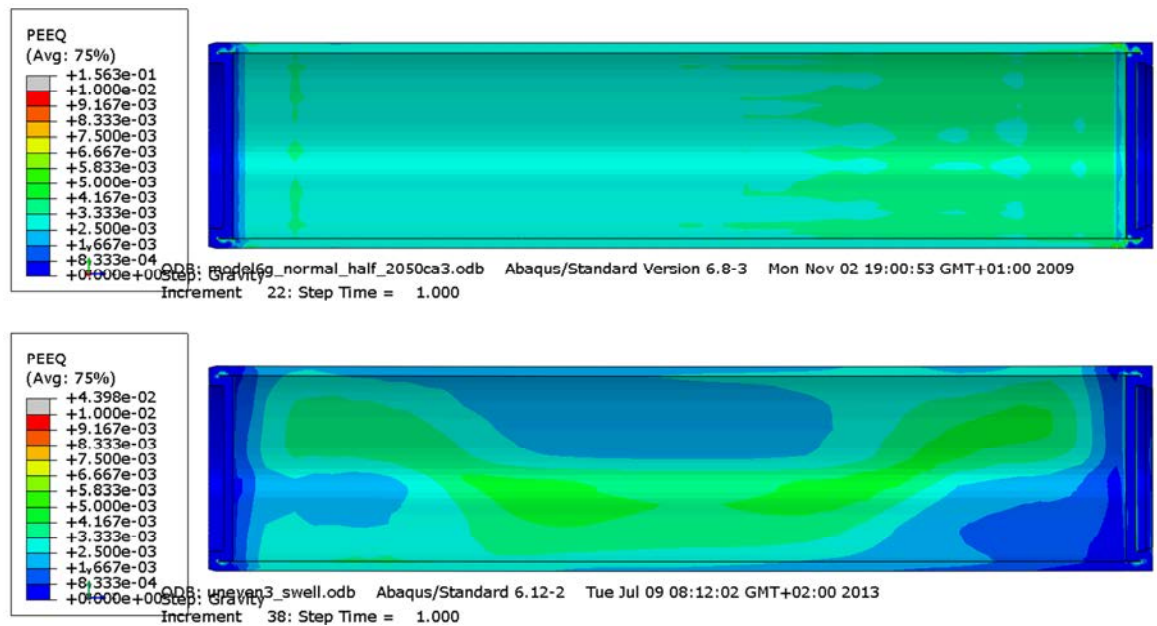
Figure 5-5. *Plastic strain in the copper shell (upper: base case).*

The results show that the stresses in the insert are as expected much higher than in the base case due to the bending effect of the uneven stresses in the buffer. The maximum principle stress is about 78 MPa, which can be compared to the analytical calculation made on the simplified model (SKBdoc 1206894) that resulted in a maximum principle stress of 111 MPa. The difference may partly be caused by the smoother stress distribution in the numerical calculation and partly by the redistribution of stresses on the copper shell to the insert. This is discussed in section 5.4.

The plastic strain in the copper shell does not differ very much between the two simulations in general, but the locally high plastization in the base case (up to 16%) is not seen in this simulation (up to 4%), the reason being the much higher swelling pressure applied in the base case.

5.3 Stresses during rock shear

5.3.1 Shear in the centre of the canister

Results after 5 and 10 cm shear are shown both as comparisons between PWR and BWR inserts and as comparisons between BWR and the base case.

Figure 5-6 shows the plastic strain in the bentonite in the two calculations with BWR and PWR inserts. As expected there is strong plastic deformation close to the shear plane and no significant differences between the two inserts.
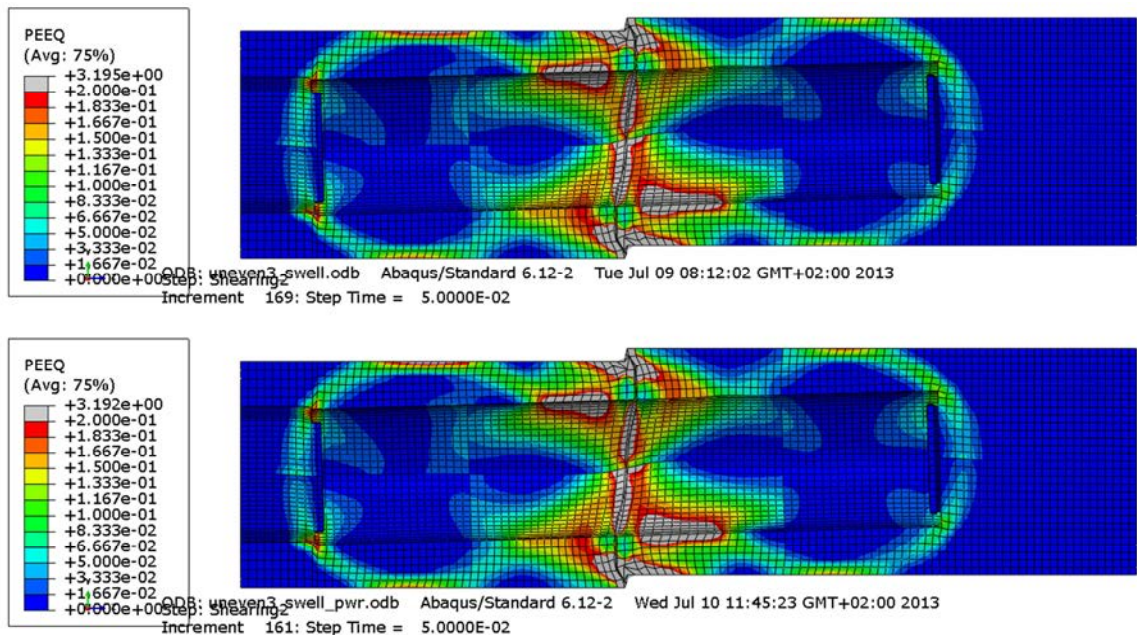
Figure 5-6. *Plastic strain in the bentonite after 10 cm shear. Upper: BWR insert; Lower PWR insert.*

Figures 5-7 to 5-10 show the plastic strain in the copper shell.

The figures and the comparison show that the plastic strain in the copper shell is lower in the new calculation with inhomogeneous buffer than in the base case. The difference is not very strong along the envelope surface but very strong in the base and the lid of the copper shell. The effect of the inhomogeneity is not enough to compensate for the higher density and swelling pressure in the base case.
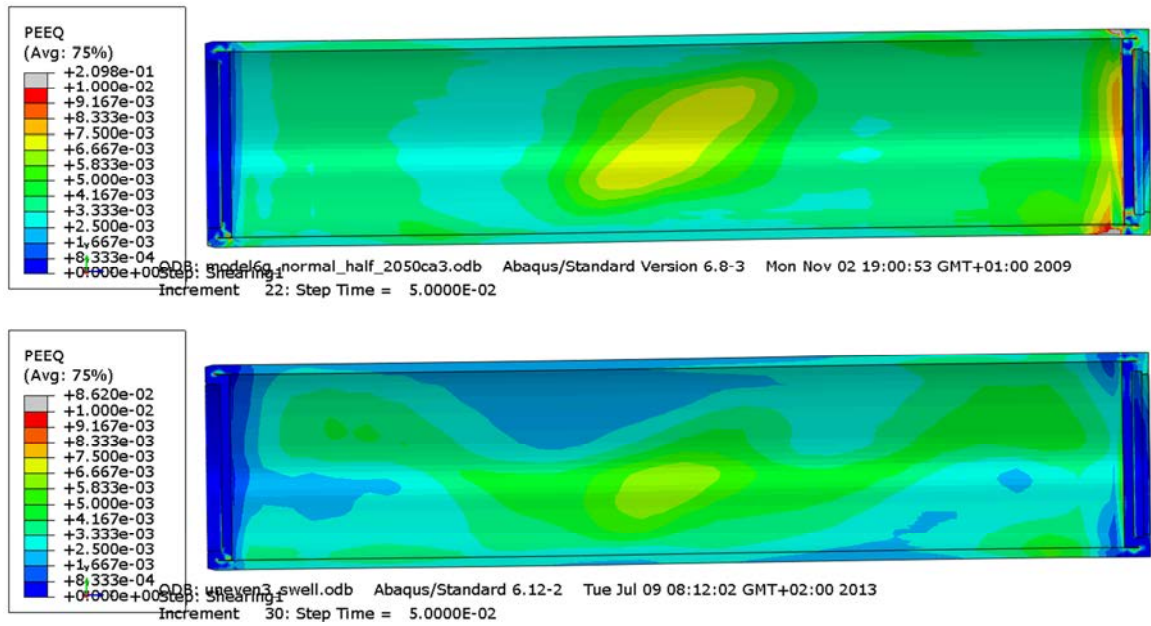
Figure 5-7. *Plastic strain in the copper shell of the BWR canister after 5 cm shear. Upper: base case.*
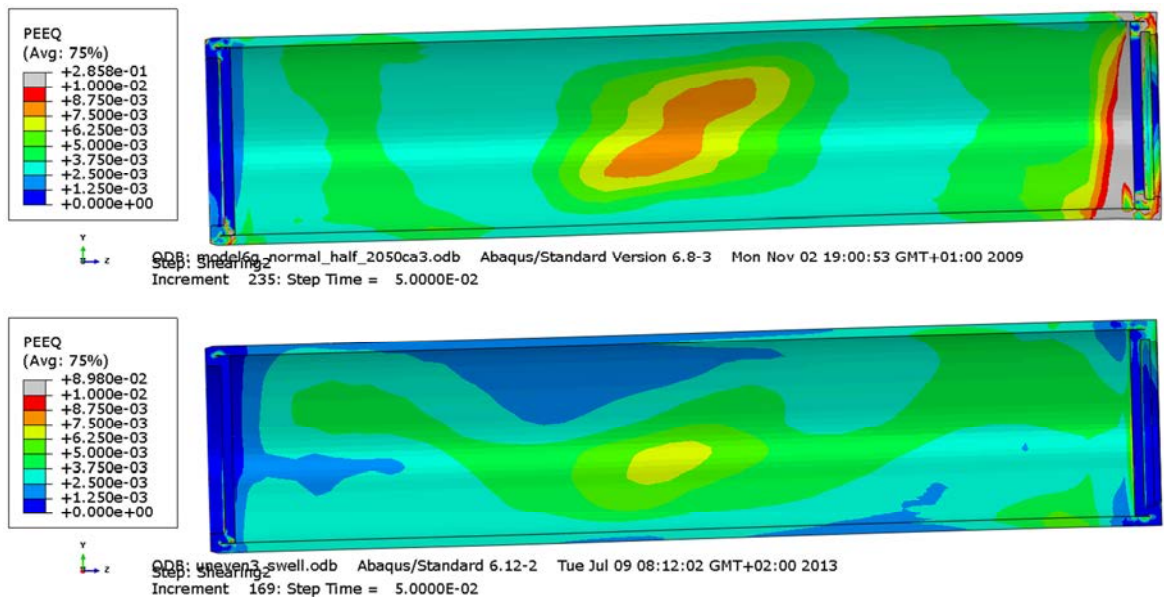

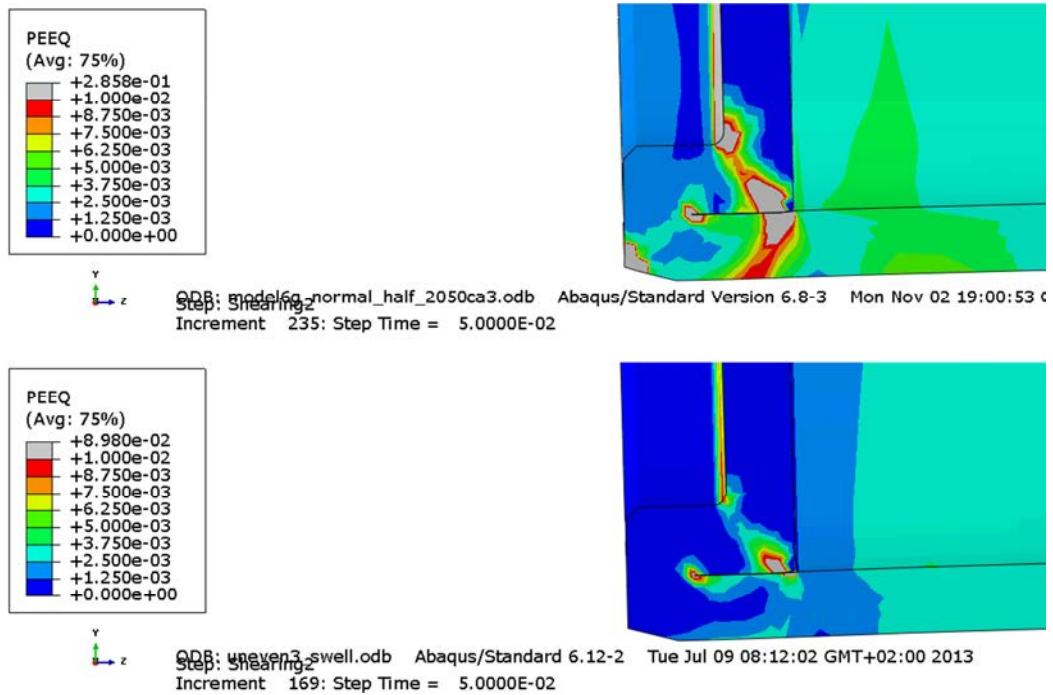**Figure 5-8.** *Plastic strain in the copper shell of the BWR canister after 10 cm shear. Upper: base case.*

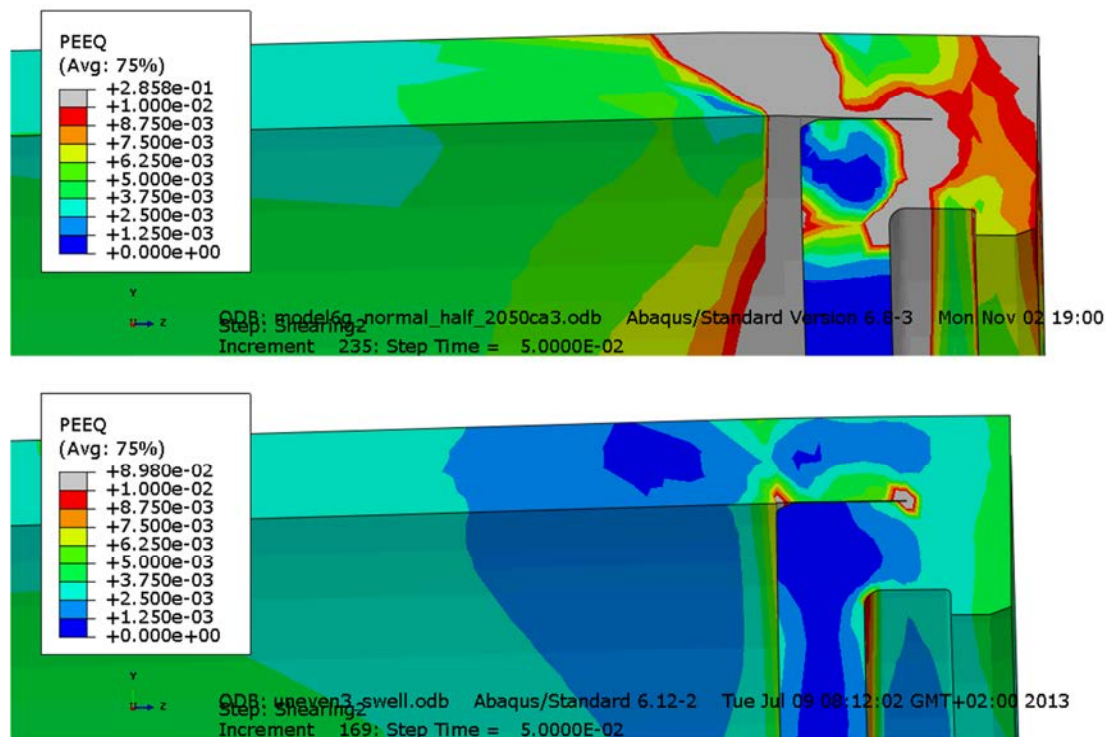**Figure 5-9**. *Details of the plastic strain in the copper shell of the BWR canister after 5 cm shear. Upper: base case.*

Figure 5-10. *Details of the plastic strain in the copper shell of the BWR canister after 10 cm shear. Upper: base case.*

The stresses in the insert are shown in Figures 5-11 to 5-15. Figure 5-11 shows Mises stresses and Figure 5-12 shows the axial stresses in both the BWR and the PWR insert after 10 cm shear.
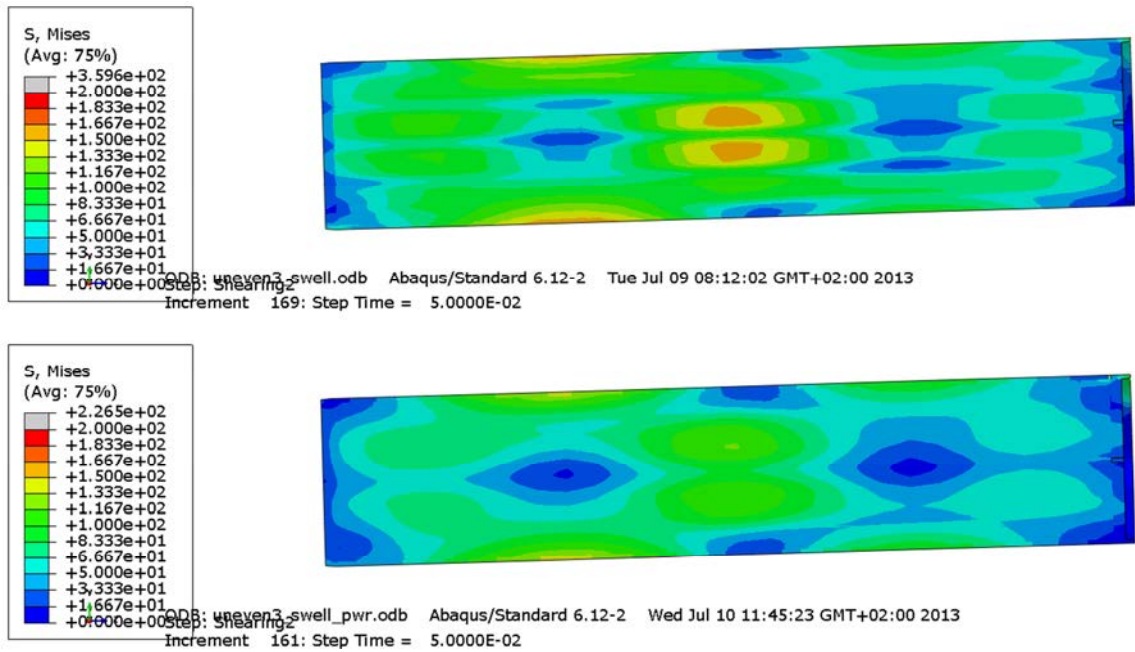

Figure 5-11. *Mises stress (MPa) in the BWR insert (upper) and in the PWR insert after 10 cm shear.*
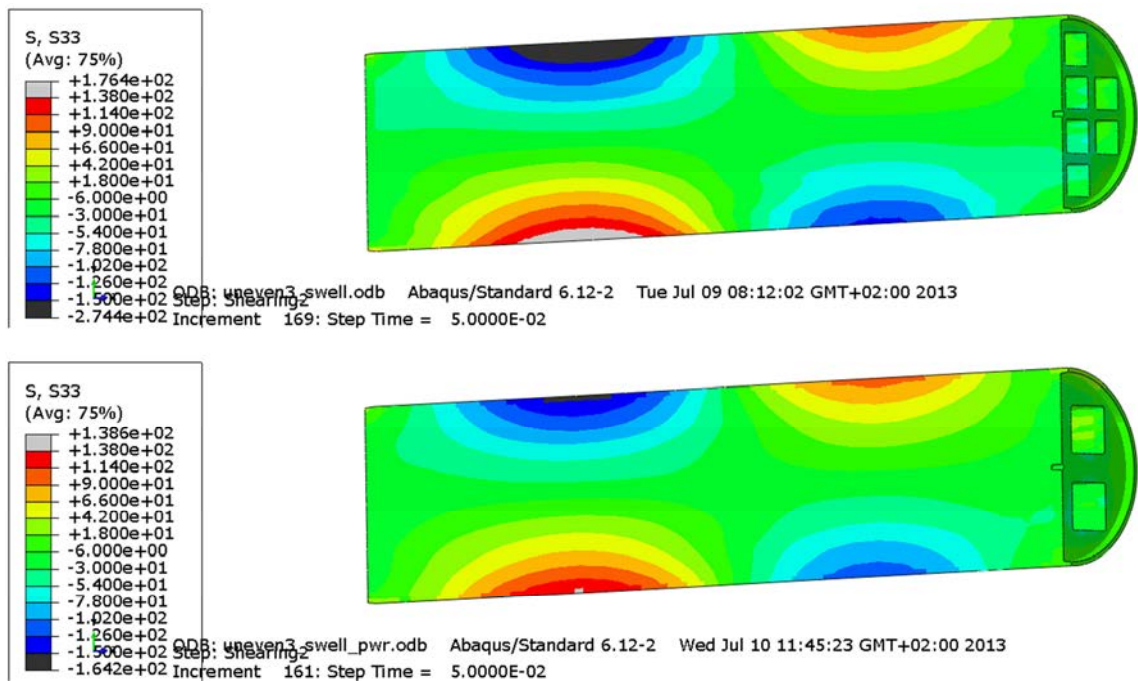

Figure 5-12. *Axial stress (MPa) in the BWR insert (upper) and in the PWR insert after 10 cm shear.*

Figures 5-13 and 5-14 show Mises stress in the BWR insert and comparison with the base case after 5 and 10 cm shear. Figure 5-15 shows a corresponding comparison for the axial stress.
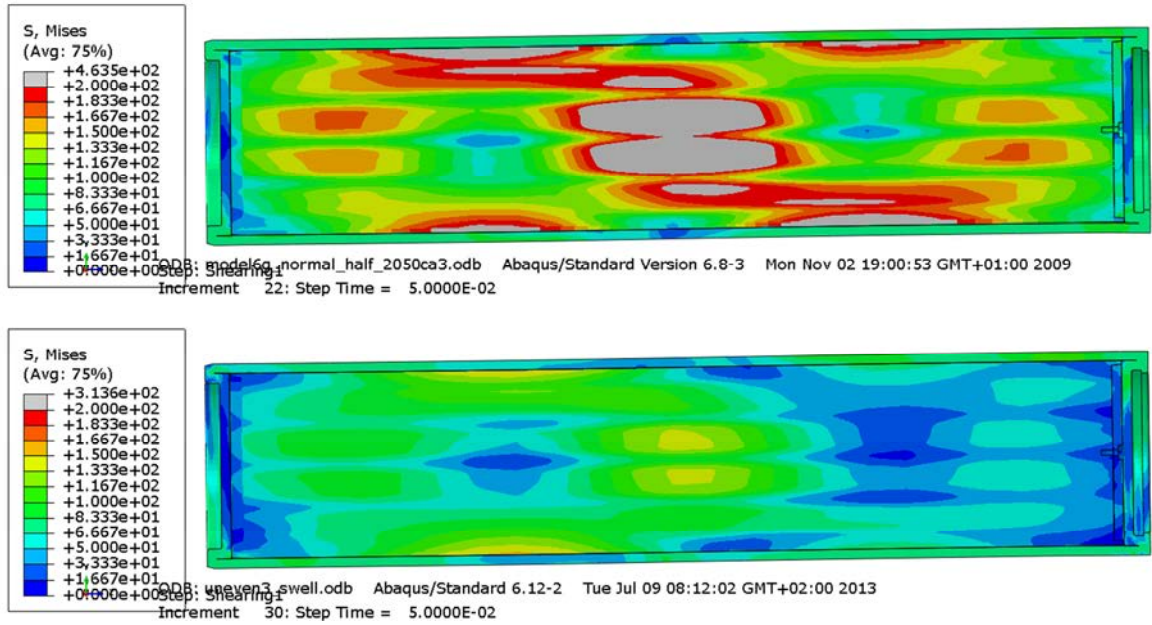

Figure 5-13. *Mises stress (MPa) in the BWR insert after 5 cm shear and comparison with the base case (upper).*
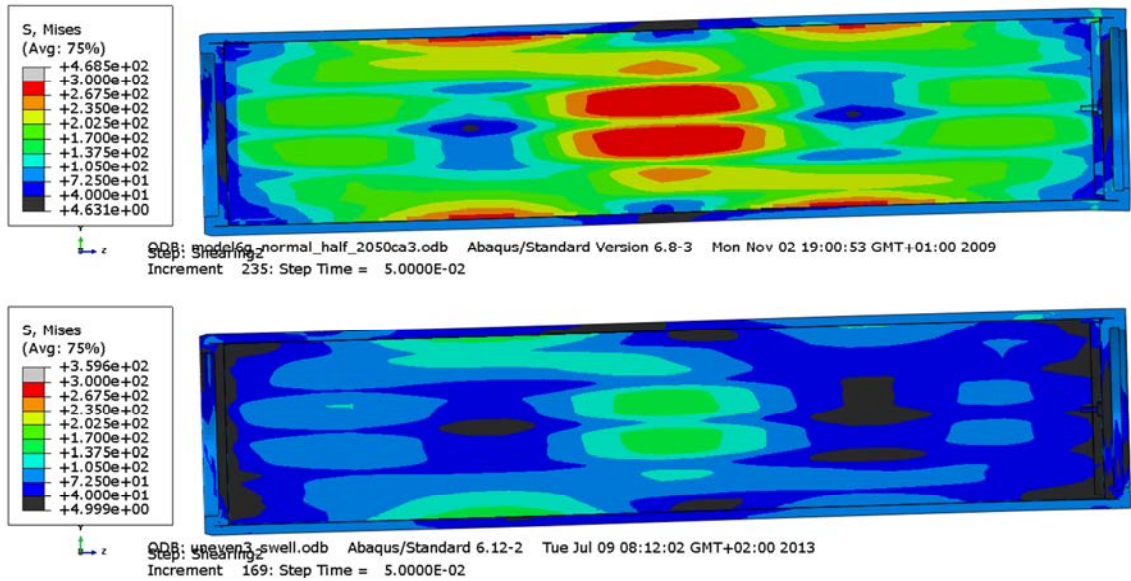

Figure 5-14. *Mises stress (MPa) in the BWR insert after 10 cm shear and comparison with the base case (upper).*
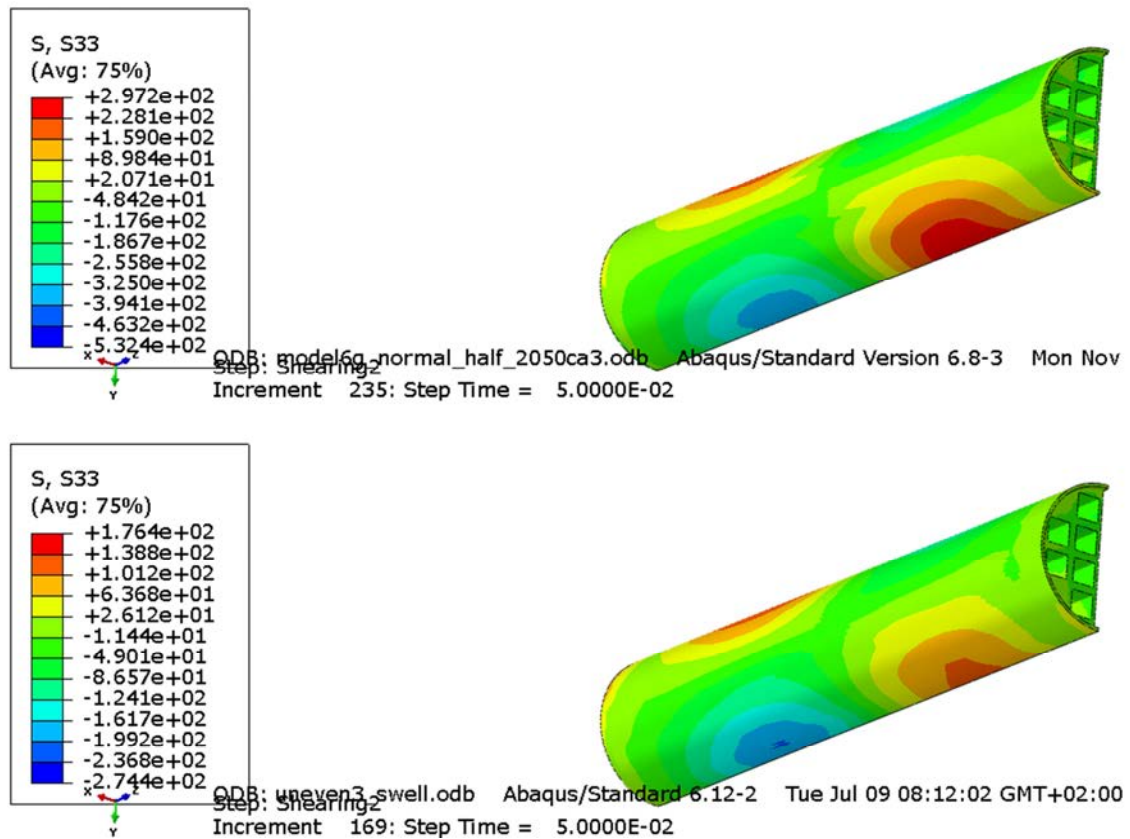
Figure 5-15. *Axial stress (MPa) in the BWR insert after 10 cm shear and comparison with the base case (upper).*

The figures and the comparison show that the stresses in the insert are lower in the new calculation with inhomogeneous buffer than in the base case. The effect of the inhomogeneity is also for the insert not enough to compensate for the higher density and swelling pressure in the base case.

5.3.2   Shear in the upper ¼-point of the canister

The same figures and comparisons will be shown for the ¼-point shear case.

Figures 5-16 to 5-19 show the plastic strain in the copper shell.

The figures and the comparison show that the plastic strain in the copper shell also for this case is lower in the new calculation with inhomogeneous buffer than in the base
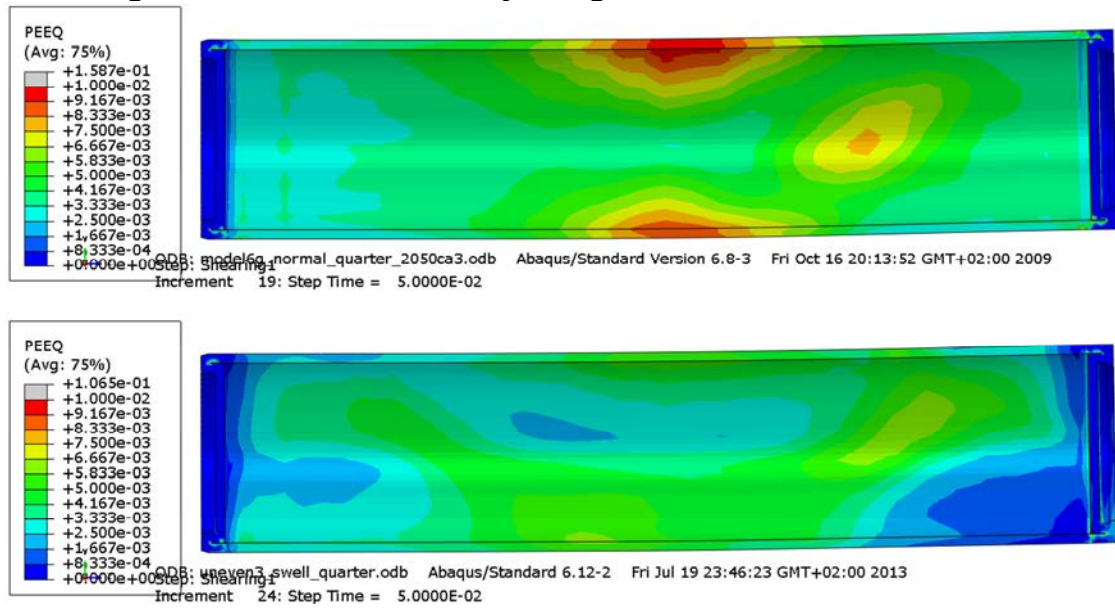
case although the differences are not very strong.

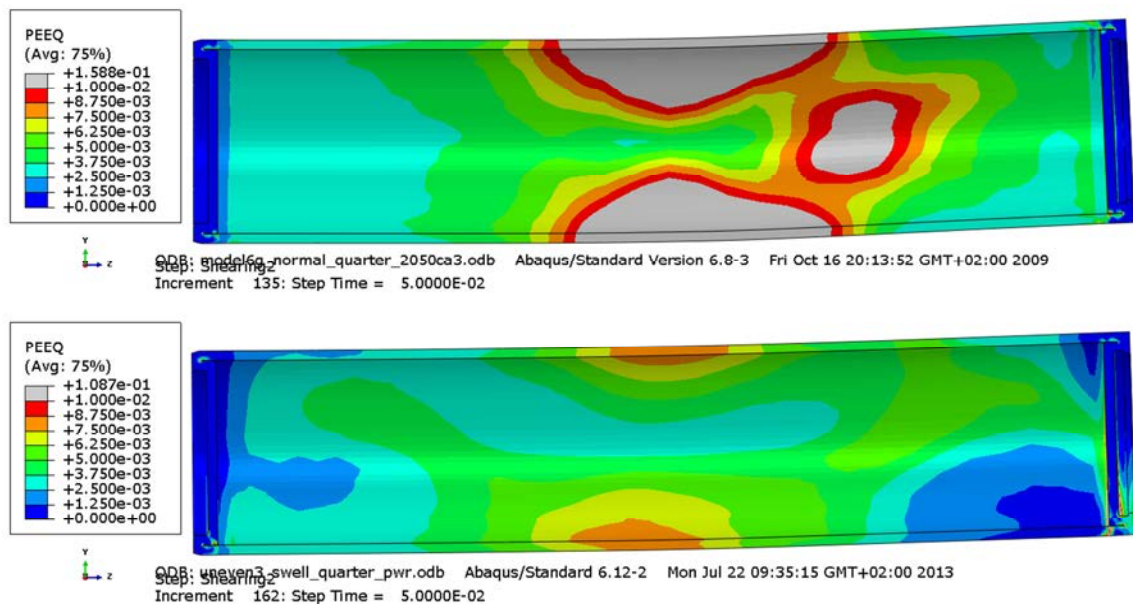**Figure 5-16.** *Plastic strain in the copper shell after 5 cm shear. Upper: base case.*

Figure 5-17. *Plastic strain in the copper shell after 10 cm shear. Upper: base case.*
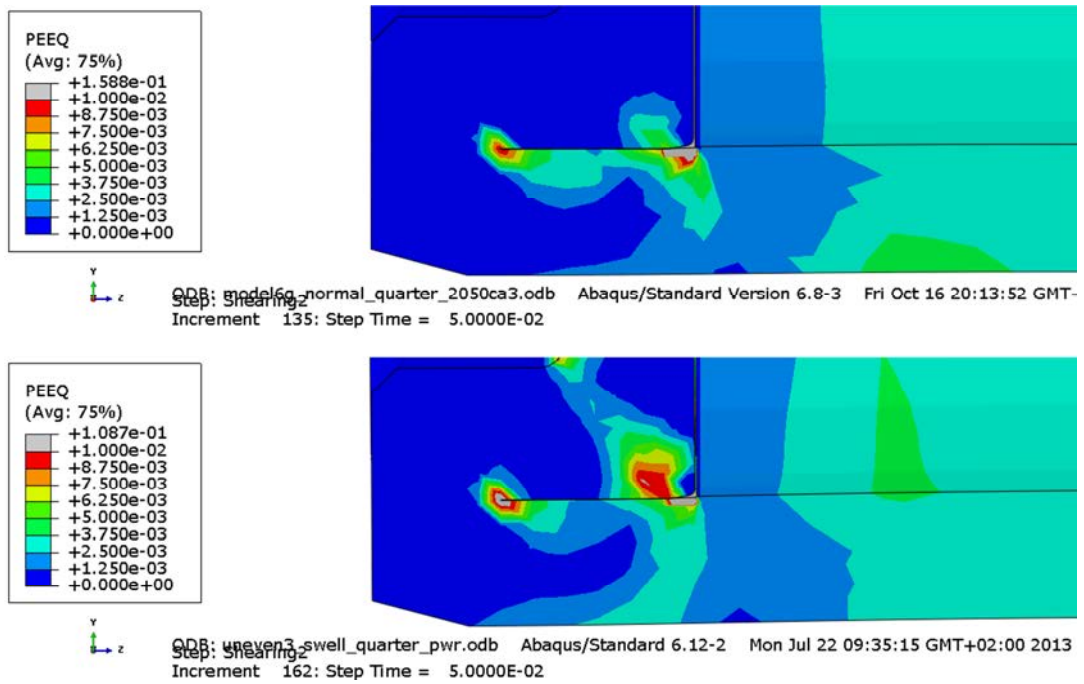
Figure 5-18. *Details of the plastic strain in the copper shell after 10 cm shear. Upper: base case.*
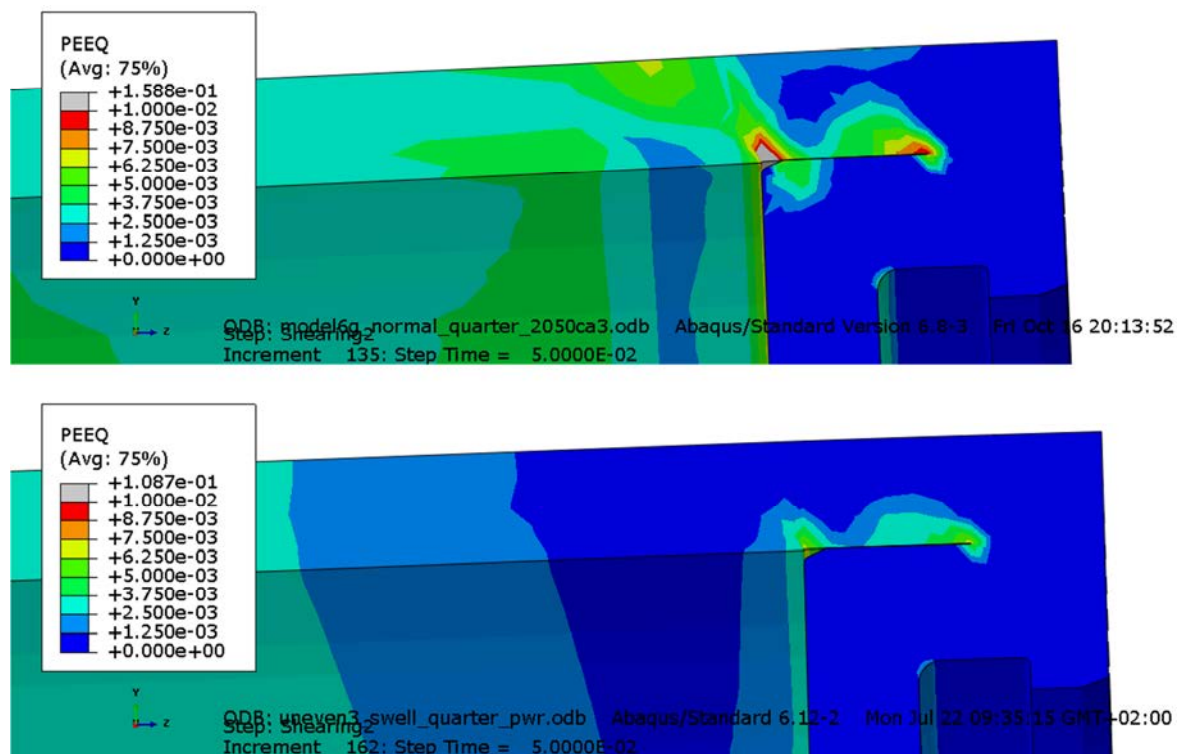

Figure 5-19. *Details of the plastic strain in the copper shell after 10 cm shear. Upper: base case.*

The stresses in the insert are shown in Figures 5-20 to 5-24. Figure 5-20 shows Mises stresses and Figure 5-21 shows the axial stresses in both the BWR and the PWR insert after 10 cm shear.
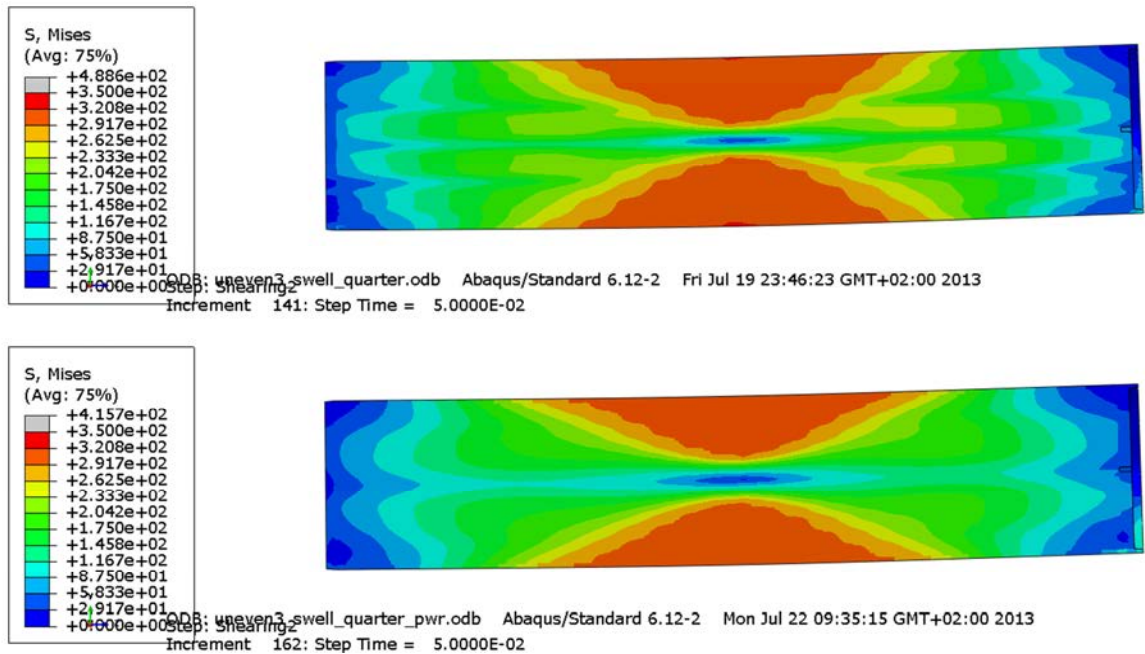

Figure 5-20. *Mises stress (MPa) in the BWR insert (upper) and in the PWR insert after 10 cm shear.*
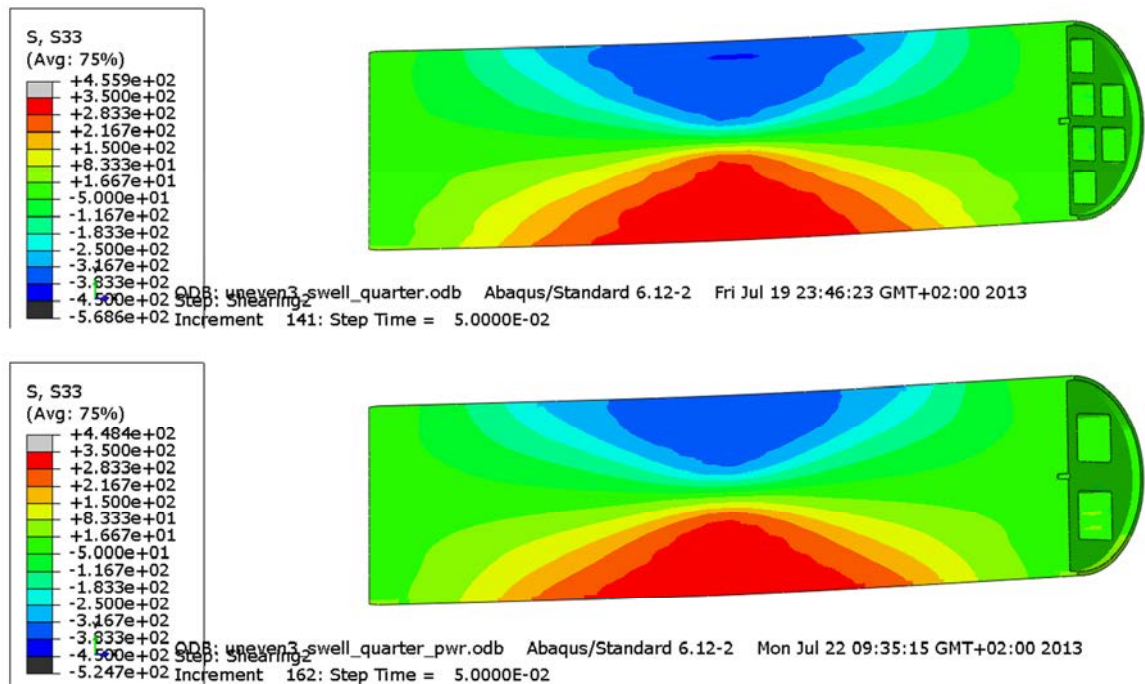
Figure 5-21. *Axial stress (MPa) in the BWR insert (upper) and in the PWR insert after 10 cm shear.*

Figures 5-22 and 5-23 show Mises stress in the BWR insert and comparison with the base case after 5 and 10 cm shear. Figure 5-24 shows a corresponding comparison for the axial stress.

Figure 5-22. *Mises stress (MPa) in the BWR insert after 5 cm shear and comparison with the base case (upper).*

Figure 5-23. *Mises stress (MPa) in the BWR insert after 10 cm shear and comparison with the base case (upper).*

Figure 5-24. Axial stress (MPa) in the BWR insert after 5 cm shear and comparison with the base case (upper).

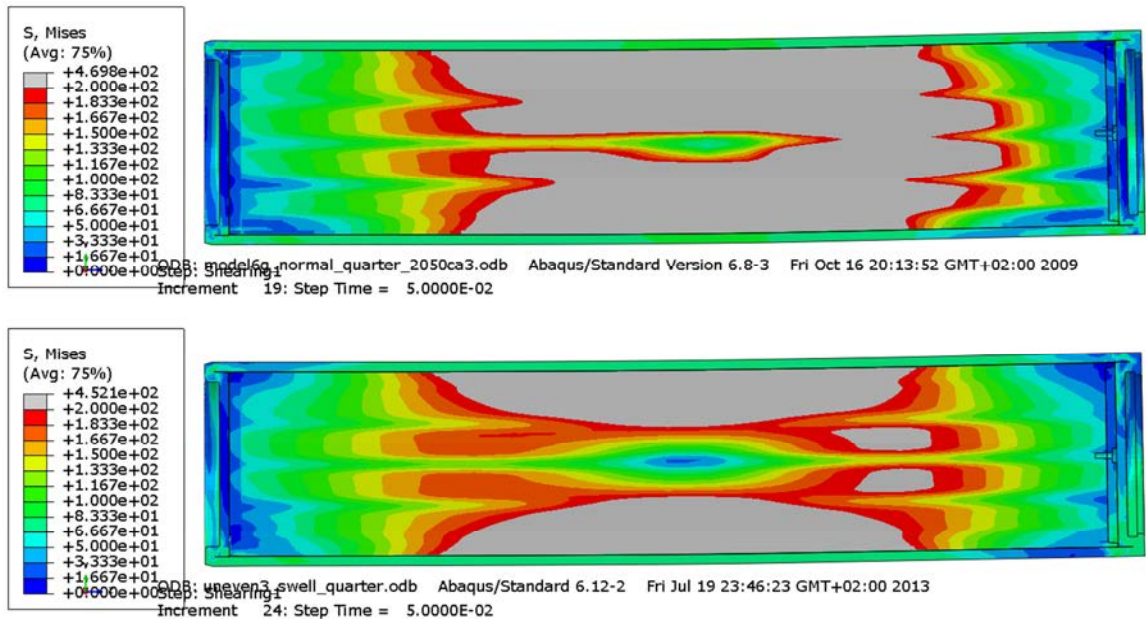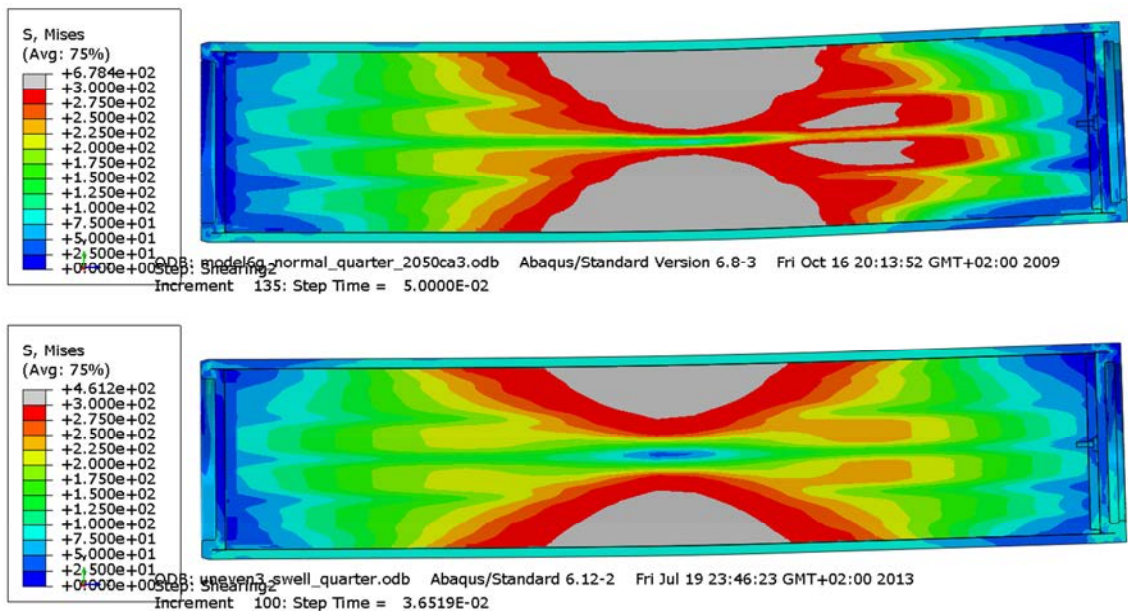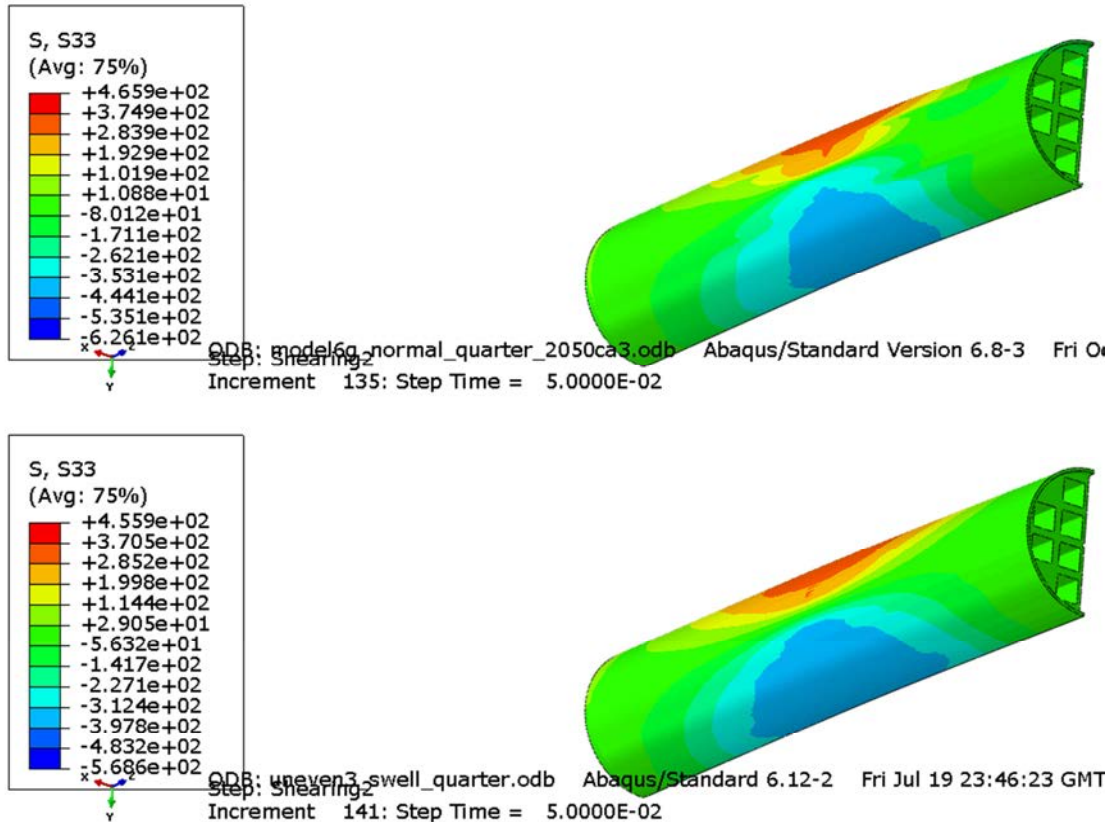The figures and the comparison show that the stresses in the insert are lower in the new calculation with inhomogeneous buffer than in the base case although the difference is very small for the axial stresses. The effect of the inhomogeneity is also for the ¼ case not enough to compensate for the higher density and swelling pressure in the base case.

5.4 Discussion

As mentioned in section 5.2 lower stresses in the insert by the inhomogeneous density distribution before shear were achieved from the numerical calculation compared to the analytical. The analytical calculation yielded a maximum axial stress of 111 MPa while the numerical yielded only 78 MPa. There are several reasons that explain such differences. One is the simplified design of the insert in the analytical case where the channel tubes are not considered. Another is the isostatic load from the water pressure 5 MPa that will reduce the tensile stresses. Of even higher importance is probably the smoother stress distribution used in the numerical calculation. However, the most important reason for the difference seems to be that the copper shell takes some of the stresses and redistributes some. Figures 5-25 illustrates this.
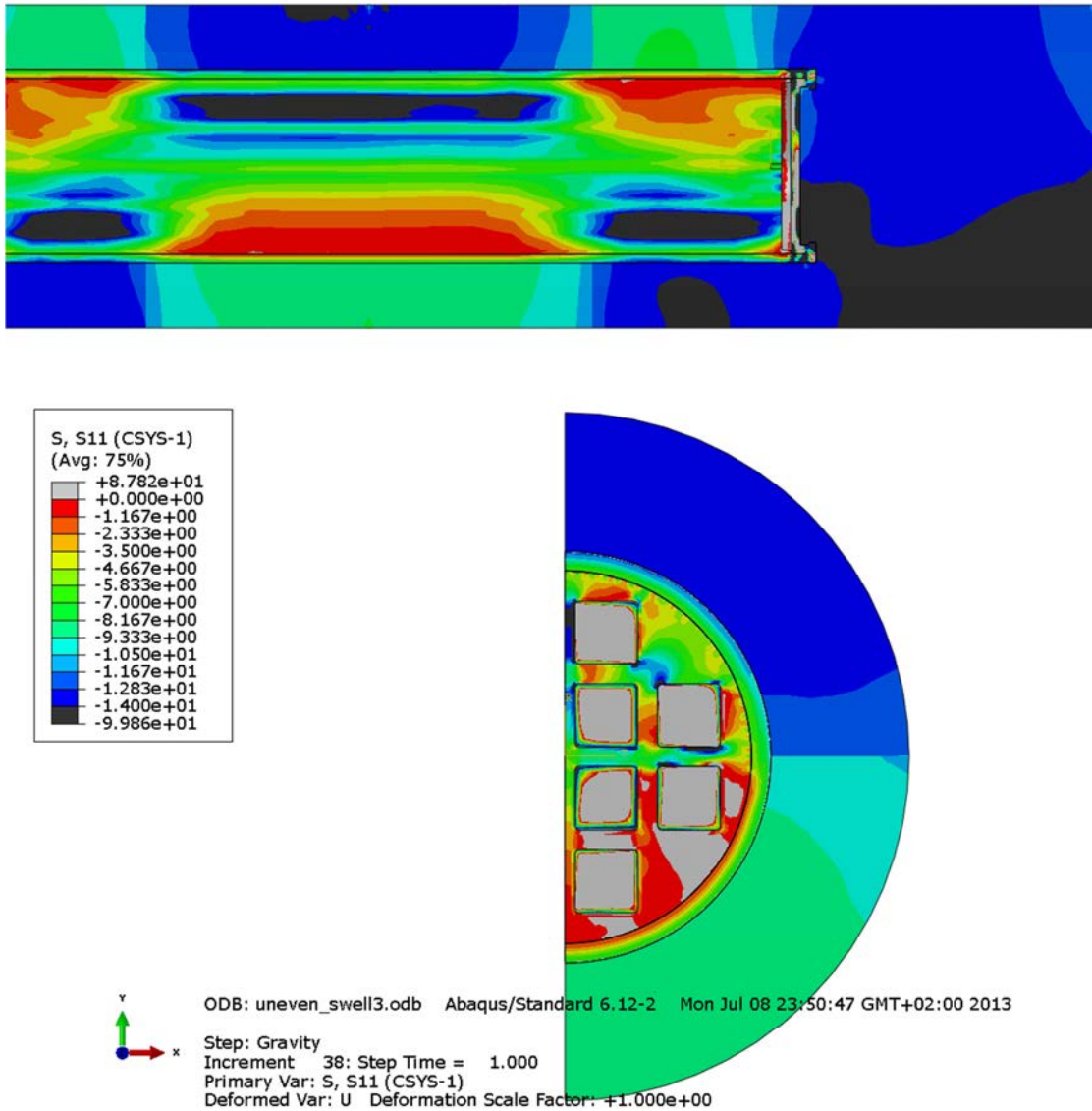
Figure 5-25. *Radial stress (MPa) in the canister.*

Figure 5-25 shows that the stresses from the bentonite are partly acting on the copper shell but not on the insert. The stresses are reduced and redistributed.

6   Conclusions

The modelling has included cast iron inserts of both PWR and BWR canisters. The uneven swelling pressure and the water pressure 5 MPa were applied as a resulting total stress in the buffer before starting the shear calculation. The material models derived for the corresponding buffer densities with rate dependant stress-strain relations were used in the shear calculations.

Two cases with horizontal shear planes and different shear plane locations have been modelled; one with the shear plane in the centre of the canister and one with the shear plane in the upper ¼-point.

The results show that the modelled case yields lower stresses in both the copper shell and the cast iron insert than the corresponding base case with the density of the buffer 2050 kg/m^3 for both PWR and BWR canisters and for both cases of shear plane location.

The maximum principle stresses in the insert before shear were about 70 MPa, which is lower than the analytical results 111 MPa. This depends mainly on the smoother stress distribution in the numerical cases than applied in the analytical calculation and on the copper shell that reduces and redistributes the stresses from the bentonite.

References

Börgesson L, Hernelind J, 2010. Earthquake induced rock shear through a deposition hole. Modelling of three model tests scaled 1:10. Verification of the bentonite material and the calculation technique. SKB TR-10-33, Svensk Kärnbränslehantering AB.

Börgesson L, Johannesson L-E, Sandén T, Hernelind J, 1995. Modelling of the physical behaviour of water saturated clay barriers. Laboratory tests, material models and finite element application. SKB TR 95-20, Svensk Kärnbränslehantering AB.

Börgesson L, Dueck A, Johannesson L-E, 2010. Material model for shear of the buffer – evaluation of laboratory test results. SKB TR-10-31, Svensk Kärnbränslehantering AB.

Dueck A, Börgesson L, Johannesson L-E, 2010. Stress-strain relation of bentonite at undrained shear. Laboratory tests to investigate the influence of material composition and test technique. SKB TR-10-32, Svensk Kärnbränslehantering AB.

Hernelind J, 2010. Modelling and analysis of canister and buffer for earthquake induced rock shear and glacial load. SKB TR-10-34, Svensk Kärnbränslehantering AB.

Jin L-Z, Sandström R, 2008. Creep of copper canisters in power-law breakdown. Computational Materials Science, 43 403–416.

Jin L-Z, Sandström R, 2009. Non-stationary creep simulation with a modified Armstrong–Frederick relation applied to copper canisters. Computational Materials Science 46, 339–346.

Karnland O, Olsson S, Nilsson U, 2006. Mineralogy and sealing properties of various bentonites and smectite-rich clay materials. SKB SKB TR-06-30, Svensk Kärnbränslehantering AB.

Raiko H, Sandström R, Rydén H, Johansson M, 2010. Design analysis report for the canister. SKB TR-10-28, Svensk Kärnbränslehantering AB.

Sandström R, Andersson H C M, 2008. Creep in phosphorus alloyed copper during power-law breakdown. Journal of Nuclear Materials 372, 76–88.

Sandström R, Hallgren J, Burman G, 2009. Stress strain flow curves for Cu-OFP. SKB R-09-14, Svensk Kärnbränslehantering AB.

SKB, 2010. Design, production and initial state of the buffer. SKB TR-10-15, Svensk Kärnbränslehantering AB.

Unpublished documents

SKBdoc id, version	Title	Issuer, year
1206894 ver 1.0	Uneven swelling pressure on the canister simplified load cases derived from uneven wetting, rock contours and buffer density distribution	SKB, 2009
1203875 ver 1.0	Ritningsförteckning för kapselkomponenter	SKB., 2009

Appendix 1 – Storage of files

This report is based on the results from FE-simulations using ABAQUS which is a commercial available code and is thus not stored as part of the work. Below is a short description of files used in the project and directories for storage of these.

1 – Input files used for the simulations

Each analysis is started by abaqus job=input-file (w/o .inp).

Contents in C:\Users\jhd\mappar\clay\ssm_questions\uneven_swelling\Model_report\Input-files

uneven3_swell	- input file with bwr-insert and mid-section shearing
uneven3_swell_pwr	- input file with pwr-insert and mid-section shearing
uneven3_swell_quarter	- input file with bwr-insert and ¼-point shearing
uneven3_swell_quarter_pwr	- input file with pwr-insert and ¼-point shearing
uneven_swell_material.incl	- material definitions
uneven_swell_pressure.incl	- initial effective pressure (model with mid-section shearing)
uneven_swell_quarter_pressure.incl	- initial effective pressure (model with ¼-point shearing)

2 – Geometry definitions

Contents in C:\Users\jhd\mappar\clay\ssm_question\uneven_swelling\Model_report\Geometry

uneven_swell.cae	- ABAQUS/CAE-database
uneven_swell.jnl	- journal file to create uneven_swell.cae (abaqus cae recover=uneven_swell.jnl)

3 – Script-files

Contents in C:\ Users\jhd\mappar\clay\ssm_question\uneven_swelling\Model_report \scripts

uneven_swell.py	- used for post-processing (abaqus cae startup=uneven_swell.py)
horizontal shearing	
compare_uneven_swell.py	– used for comparison plots
mesh.py	– script for generating mesh plots
amplitudes_start.py	- script for generating initial pressure (abaqus python
amplitude_start.py job uneven_swell	
amplitude.py	- script called by amplitude_starts.py

4 – Plots

Contents in C:\ Users\jhd\mappar\clay\ssm_question\uneven_swelling\Model_report \plots

compare-s33_max.png
compare_bentonite_peeq.png
compare_bwr-copper_peeq_10cm.png
compare_bwr-copper_peeq_10cm_detail1.png
compare_bwr-copper_peeq_10cm_detail2.png
compare_bwr-copper_peeq_10cm_detail4.png
compare_bwr-copper_peeq_5cm.png
compare_bwr-copper_peeq_detail1_10cm.png
compare_bwr-copper_peeq_detail2_10cm.png
compare_bwr-copper_peeq_detail4_10cm.png
compare_bwr-copper_peeq_gravity.png
compare_bwr-insert_mises_gravity.png
compare_bwr-insert_s33_10cm.png
compare_bwr-insert_s33_gravity.png
compare_bwr-insert_sprin_max_gravity.png
compare_bwr-mises_10cm.png
compare_bwr-mises_5cm.png
compare_bwr-mises_gravity.png
compare_copper_mises.png
compare_copper_peeq.png
compare_insert_mises.png
compare_insert_s33.png
compare_quarter_bentonite_peeq.png
compare_quarter_bwr-copper_peeq_10cm.png
compare_quarter_bwr-copper_peeq_10cm_detail1.png
compare_quarter_bwr-copper_peeq_10cm_detail2.png
compare_quarter_bwr-copper_peeq_10cm_detail4.png
compare_quarter_bwr-copper_peeq_5cm.png
compare_quarter_bwr-copper_peeq_gravity.png
compare_quarter_bwr-insert_mises_gravity.png
compare_quarter_bwr-insert_s33_10cm.png
compare_quarter_bwr-insert_s33_gravity.png
compare_quarter_bwr-insert_sprin_max_gravity.png
compare_quarter_bwr-mises_10cm.png
compare_quarter_bwr-mises_5cm.png
compare_quarter_bwr-mises_gravity.png
compare_quarter_copper_mises.png
compare_quarter_copper_peeq.png
compare_quarter_insert_mises.png
compare_quarter_insert_s33.png
initial_pressure.png
uneven3_swell_pwr-model_insert.png
uneven3_swell_quarter-model.png
uneven3_swell_quarter-model_buffer.png
uneven3_swell_quarter-model_copper.png
uneven3_swell_quarter-model_insert_bwr.png
uneven3_swell_quarter-model_lid.png
uneven3_swell_quarter-radial stress_midsection.png
uneven3_swell_quarter-radial stress_symmetry.png
uneven_swell-compare_s33_insert_end.png
uneven_swell-cpress.png
uneven_swell-cpress_analysis.png
uneven_swell-cpress_analysis_end.png
uneven_swell-mises_insert_end.png
uneven_swell-peeq_bentonite_end.png
uneven_swell-peeq_copper_end.png
uneven_swell-s33_insert_end.png
uneven_swell3-model.png
uneven_swell3-model_buffer.png
uneven_swell3-model_copper.png
uneven_swell3-model_insert-pwr.png
uneven_swell3-model_insert_bwr.png
uneven_swell3-model_lid.png
uneven_swell3-radial stress_midsection.png
uneven_swell3-radial stress_symmetry.png